The Geological Society of America
Special Paper 438
2008

The Ingalls ophiolite complex, central Cascades, Washington: Geochemistry, tectonic setting, and regional correlations

James H. MacDonald Jr.[†]
Gregory D. Harper
Department of Earth and Atmospheric Sciences, State University of New York, Albany, New York 12222-0001, USA

Robert B. Miller
Jonathan S. Miller
Ante N. Mlinarevic
Cynthia E. Schultz
Department of Geology, San Jose State University, San Jose, California 95192-0102, USA

ABSTRACT

The polygenetic Ingalls ophiolite complex in the central Cascades, Washington, is one of several Middle to Late Jurassic ophiolites of the North American Cordillera. It consists primarily of mantle tectonites. High-temperature mylonitic peridotite, overprinted by serpentinite mélange (Navaho Divide fault zone), separates harzburgite and dunite in the south from lherzolite in the north. Crustal units of the ophiolite occur as steeply dipping, kilometer-scale fault blocks within the Navaho Divide fault zone. These units are the Iron Mountain, Esmeralda Peaks, and Ingalls sedimentary rocks.

Volcanic rocks of the Iron Mountain unit have transitional within-plate–enriched mid-ocean-ridge basalt affinities, and a rhyolite yields a U-Pb zircon age of ca. 192 Ma. Minor sedimentary rocks include local oolitic limestones and cherts that contain Lower Jurassic (Pliensbachian) Radiolaria. This unit probably formed as a seamount within close proximity to a spreading ridge. The Esmeralda Peaks unit forms the crustal section of the ophiolite, and it consists of gabbro, diabase, basalt, lesser felsic volcanics, and minor sedimentary rocks. U-Pb zircon indicates that the age of this unit is ca. 161 Ma. The Esmeralda Peaks unit has transitional island-arc–mid-ocean ridge basalt and minor boninitic affinities. A preferred interpretation for this unit is that it formed initially by forearc rifting that evolved into back-arc spreading, and it was subsequently deformed by a fracture zone. The Iron Mountain unit is the rifted basement of the Esmeralda Peaks unit, indicating that the Ingalls ophiolite complex is polygenetic. Ingalls sedimentary rocks consist primarily of argillite with minor graywacke, conglomerate, chert, and ophiolite-derived breccias and olistoliths. Radiolaria from chert give lower Oxfordian ages.

[†]Department of Marine and Ecological Sciences, Florida Gulf Coast University, 10501 FGCU Boulevard, South, Fort Myers, Florida 33965, USA; e-mail: jmacdona@fgcu.edu.

MacDonald, J.H., Jr., Harper, G.D., Miller, R.B., Miller, J.S., Mlinarevic, A.N., and Schultz, C.E., 2008, The Ingalls ophiolite complex, central Cascades, Washington: Geochemistry, tectonic setting, and regional correlations, *in* Wright, J.E., and Shervais, J.W., eds., Ophiolites, Arcs, and Batholiths: A Tribute to Cliff Hopson: Geological Society of America Special Paper 438, p. 133–159, doi: 10.1130/2008.2438(04). For permission to copy, contact editing@geosociety.org.

The Ingalls ophiolite complex is similar in age and geochemistry to the Josephine ophiolite and its related rift-edge facies and to the Coast Range ophiolite of California and Oregon. The Ingalls and Josephine ophiolites are polygenetic, while the Coast Range ophiolite is not, and sedimentary rocks (Galice Formation) that sit on the Josephine and its rift-edge facies have the same Radiolaria fauna as Ingalls sedimentary rocks. Therefore, we correlate the Ingalls ophiolite complex with the Josephine ophiolite of the Klamath Mountains. Taking known Cretaceous and younger strike-slip faulting into account, this correlation implies that the Josephine ophiolite either continued northward ~440 km—thus increasing the known length of the Josephine basin—or that the Ingalls ophiolite was translated northward ~440 km along the continental margin.

Keywords: Ingalls, Josephine, Coast Range, ophiolite, Jurassic.

INTRODUCTION

Seafloor rifting and spreading within suprasubduction zones occurs in the western Pacific island arcs and in the East Scotia Sea in the southern Atlantic (e.g., Stern, 2002; Hawkins, 2003; Livermore, 2003; Martinez and Taylor, 2003). Seafloor spreading within these suprasubduction zones can start either synchronously with arc formation (Scotia Sea; Larter et al., 2003) or by rifting of a previously active arc (Lau and Mariana Basins; Hawkins, 1995, 2003; Martinez and Taylor, 2003). Rifting within the forearc also occurs in the suprasubduction-zone environment (Bloomer, 1983; Bloomer and Hawkins, 1983; Hawkins and Melchior, 1985). The suprasubduction-zone setting is considered to be a likely place of origin for many, if not most, ophiolites (Dewey and Bird, 1971; Miyashiro, 1973; Pearce et al., 1984, Hawkins, 1995, 2003; Shervais, 2001; Pearce, 2003), including the belt of Middle to Late Jurassic ophiolites in the western United States (Fig. 1). These Cordilleran ophiolites have been proposed to represent oceanic crust formed by extension in a variety of suprasubduction-zone settings, including back-arc or forearc spreading and rifting of arc or forearc crust (Harper, 1984, 2003a; Harper and Wright, 1984; Wyld and Wright, 1988; Dilek, 1989a, 1989b; Saleeby, 1992; Stern and Bloomer, 1992; Miller et al., 1993; Harper et al., 1994, 2003; Dickinson et al., 1996; Metzger et al., 2002; Shervais et al., 2005a, 2005b). The origin for some of these ophiolites remains controversial (e.g., Coast Range ophiolite; Fig. 1) (Dickinson et al., 1996; Shervais, 2001; Shervais et al., 2004, 2005a; Hopson et al., this volume), while others are better constrained (e.g., Josephine ophiolite; Fig. 1) (Harper, 1984, 2003a, 2003b; Harper and Wright, 1984; Harper et al., 1994; Wyld and Wright, 1988).

The Ingalls ophiolite complex, located within Washington State (Fig. 1), is a northern continuation of this Jurassic Cordilleran ophiolite belt. Understanding of the tectonic origin of the Ingalls ophiolite complex is critical in understanding the Jurassic tectonic evolution of the North American Cordillera. This ophiolite has had various tectonic settings proposed for its origin. Southwick (1974) suggested that the plutonic rocks formed in a marginal basin or open ocean, whereas the volcanic and sedimentary rocks originated in an island arc. Miller and colleagues

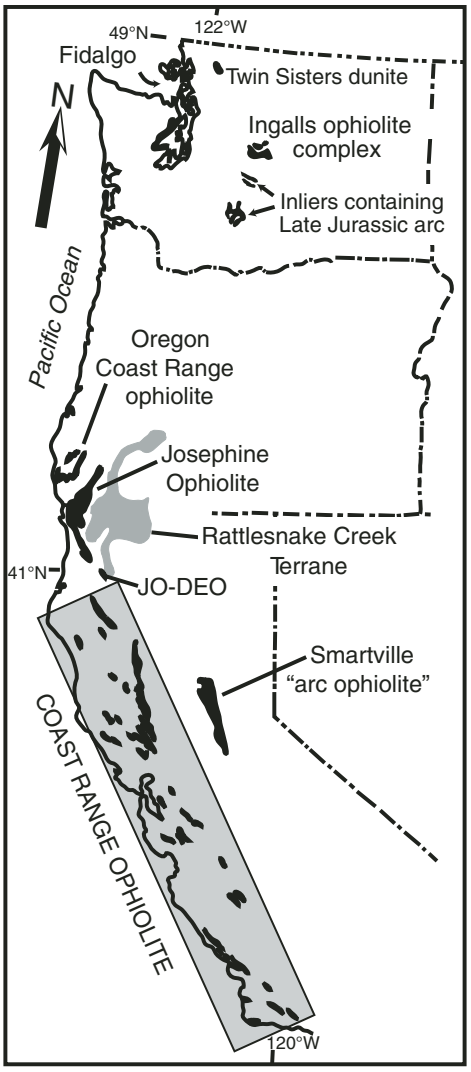

Figure 1. Location of the Middle to Late Jurassic North American Cordilleran ophiolites and the older Rattlesnake Creek terrane. Figure was modified from Miller et al. (1993) and Metzger et al. (2002). Names of the inliers containing the Late Jurassic arc complexes are, from north to south, Hicks Butte, Manastash, and Rimrock Lake (Miller, 1989; Miller et al., 1993). JO-DEO—Devils Elbow ophiolite.

(Miller, 1985; Miller and Mogk, 1987; Miller et al., 1993) concluded that the Ingalls ophiolite complex was a fracture-zone ophiolite that originated in a back-arc basin. Metzger et al. (2002) noted that most of the geochemical affinities of the mafic rocks of the Ingalls ophiolite complex supported this back-arc basin setting, but other mafic rocks had geochemical affinities of within-plate tectonic settings. In this paper, we present new geological and geochemical data documenting a polygenetic origin for the ophiolite, and we demonstrate that the complex contains an older mafic unit (Iron Mountain unit) that has within-plate magmatic affinities. These new data are used to compare the Ingalls ophiolite complex with other Cordilleran ophiolites (Fig. 1) and provide regional correlations that can help to constrain the Jurassic evolution of the North American Cordillera.

INGALLS OPHIOLITE COMPLEX

The Ingalls ophiolite complex, located within the Northwest Cascade System (e.g., Misch, 1966; Brown, 1987; Brandon et al., 1988), is the largest (450 km^2) and most complete ophiolite within Washington State (Fig. 1). This ophiolite complex is intruded by the 91–96.5 Ma Mount Stuart batholith (Miller et al., 2003; Matzel et al., 2006) and is overlain by Eocene sedimentary rocks to the south (Figs. 2 and 3). The Ingalls ophiolite complex has been dextrally faulted to the south ≥90 km along the Eocene Straight Creek fault (Misch, 1977; Miller et al., 1993; Tabor, 1994; MacDonald, 2006).

The Ingalls ophiolite complex has been thrust over the Cascade crystalline core along the Cretaceous Windy Pass thrust

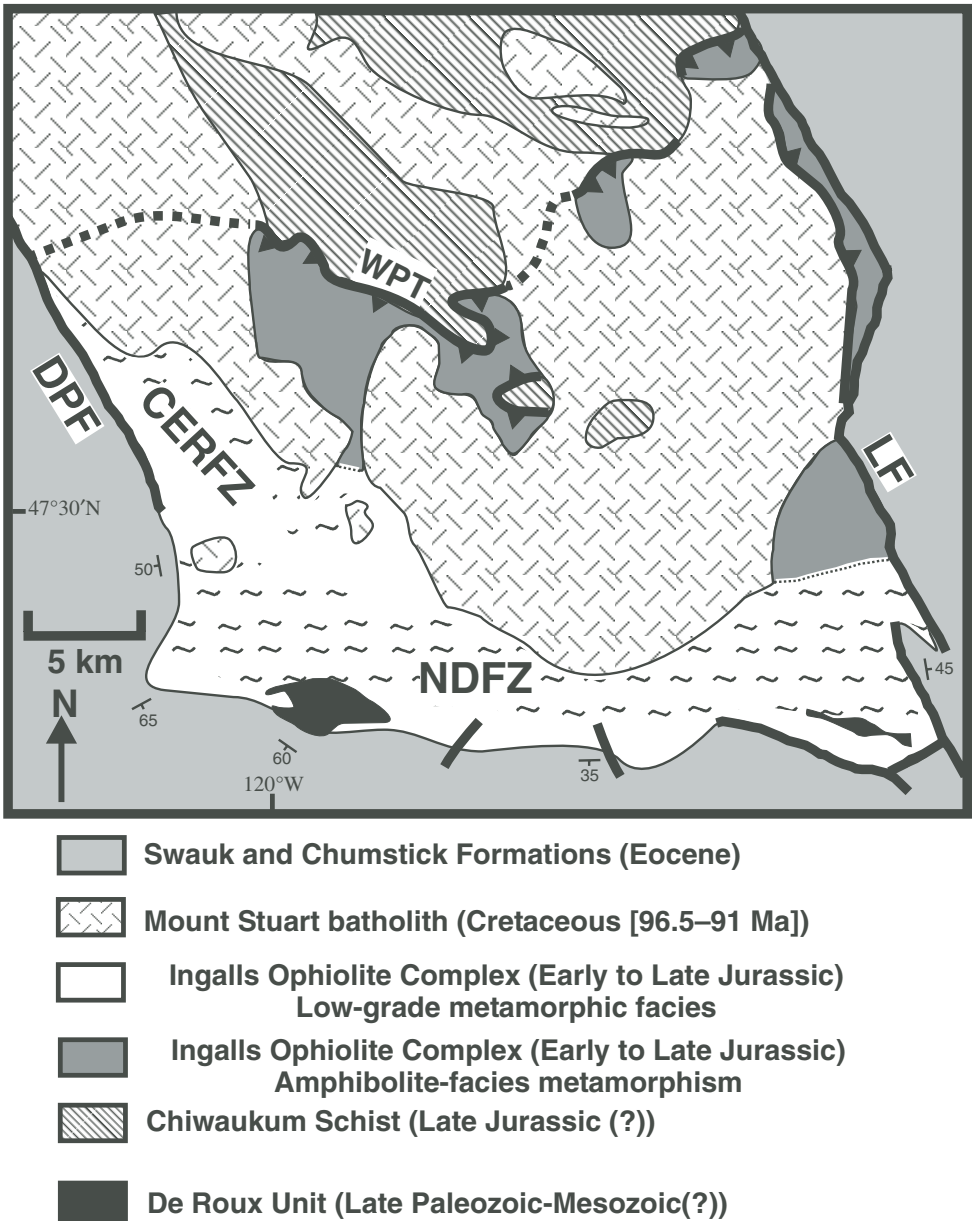

Figure 2. Map of the Ingalls ophiolite complex, surrounding units, and major structures. Figure was modified from Miller (1980) and Tabor and collaborators (1982, 1987, 1993, 2000). CERFZ—Cle Elum Ridge fault zone; DPF—Deception Pass fault; LF—Leavenworth fault; NDFZ—Navaho Divide fault zone; WPT—Windy Pass thrust.

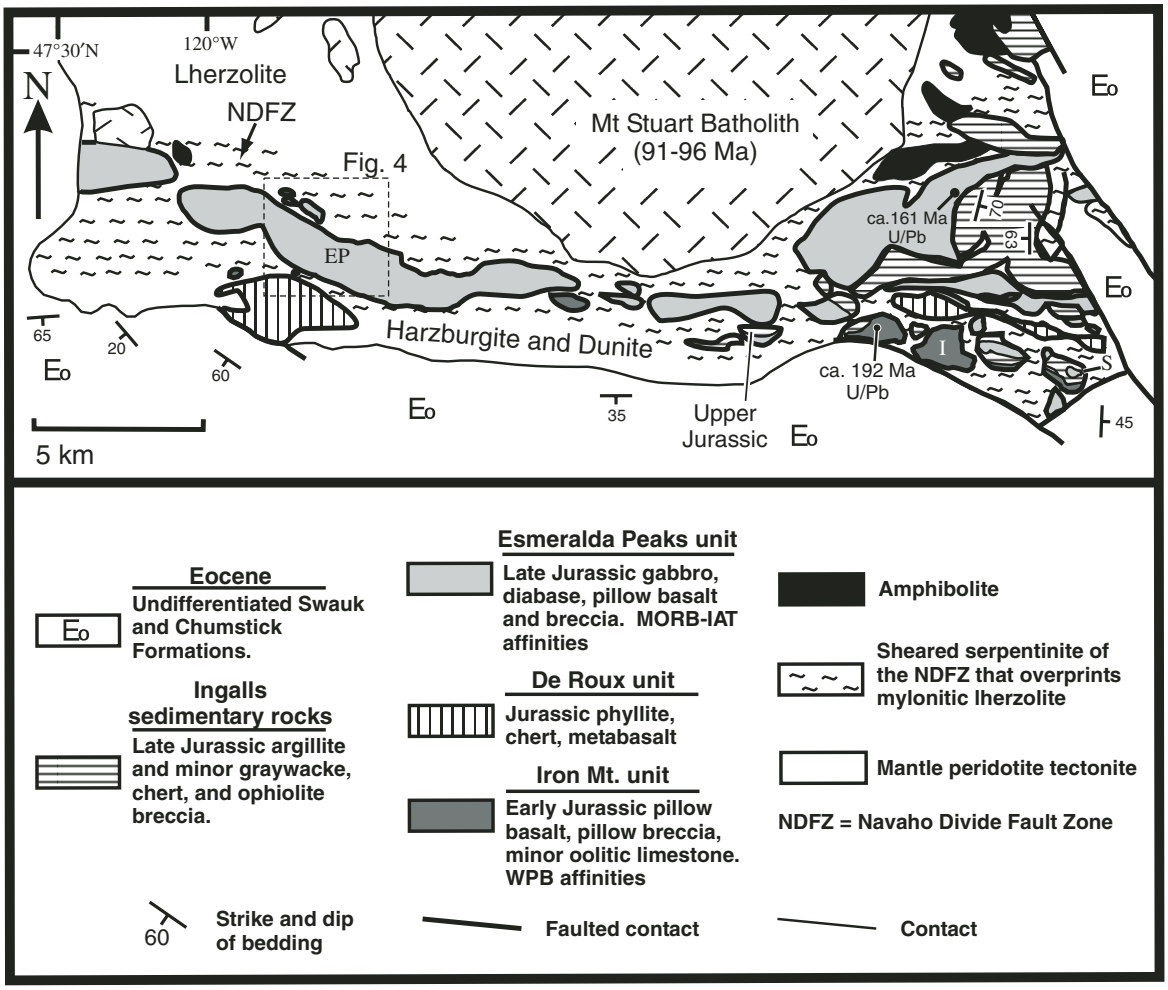

Figure 3. Map showing the mafic units of the Ingalls ophiolite complex and the unrelated De Roux unit. Figure was modified from Tabor and collaborators (1982, 1987, 1993, 2000) and Harper et al. (2003). EP—location of Esmeralda Peaks; I—location of Iron Mountain; S—location of Sheep Mountain. IAT—island-arc tholeiite; WPB—within-plate basalt; MORB—mid-ocean-ridge basalt.

(Fig. 2; Miller, 1980, 1985). The major internal structures of the ophiolite are two east-west–striking zones of serpentinite mélange (Navaho Divide and Cle Elum Ridge fault zones; Fig. 2) (Pratt, 1958; Frost, 1973; Miller, 1980, 1985).

Wyld et al. (2006), using palinspastic reconstructions, proposed that the ophiolite complex was dextrally faulted between 300 and 800 km before the Cretaceous; other researchers, using paleomagnetic data from the Mount Stuart batholith and other units in the northern Cordillera, have suggested that the Ingalls rocks have been translated as much as 3000 km from the south (Baja British Columbia hypothesis; Beck et al., 1981; Ague and Brandon, 1996; Housen et al., 2003).

The Ingalls ophiolite complex consists predominantly of variably serpentinized peridotite of upper mantle origin with lesser mafic plutonic and volcanic rocks, and minor sedimentary rocks (Fig. 3; Miller, 1980, 1985). Although the plutonic, volcanic, and sedimentary rocks all occur as fault-bounded blocks within serpentinite mélange of the Navaho Divide fault zone (Fig. 3), a nearly complete ophiolite "stratigraphy" can be recognized internally within the faulted blocks (Miller, 1980, 1985).

Mantle Units

Over two-thirds of the Ingalls ophiolite complex consists of ultramafic tectonites, representing the residual peridotite left after extraction of a mafic melt (Fig. 3; Miller, 1985; Miller and Mogk, 1987; Schultz et al., 2005). Miller (1985) recognized three mantle units within the peridotites. Mylonitic lherzolite and hornblende peridotite occur within and up to a few kilometers north of the serpentinite mélange of the Navaho Divide fault zone. Lherzolite and clinopyroxene-bearing harzburgite, with minor plagioclase peridotite and dunite, are exposed north of the mylonitic ultramafites (Figs. 3 and 4; Miller, 1980, 1985; Miller and Mogk, 1987). Harzburgite, cut by numerous bodies of dunite, some of which contain

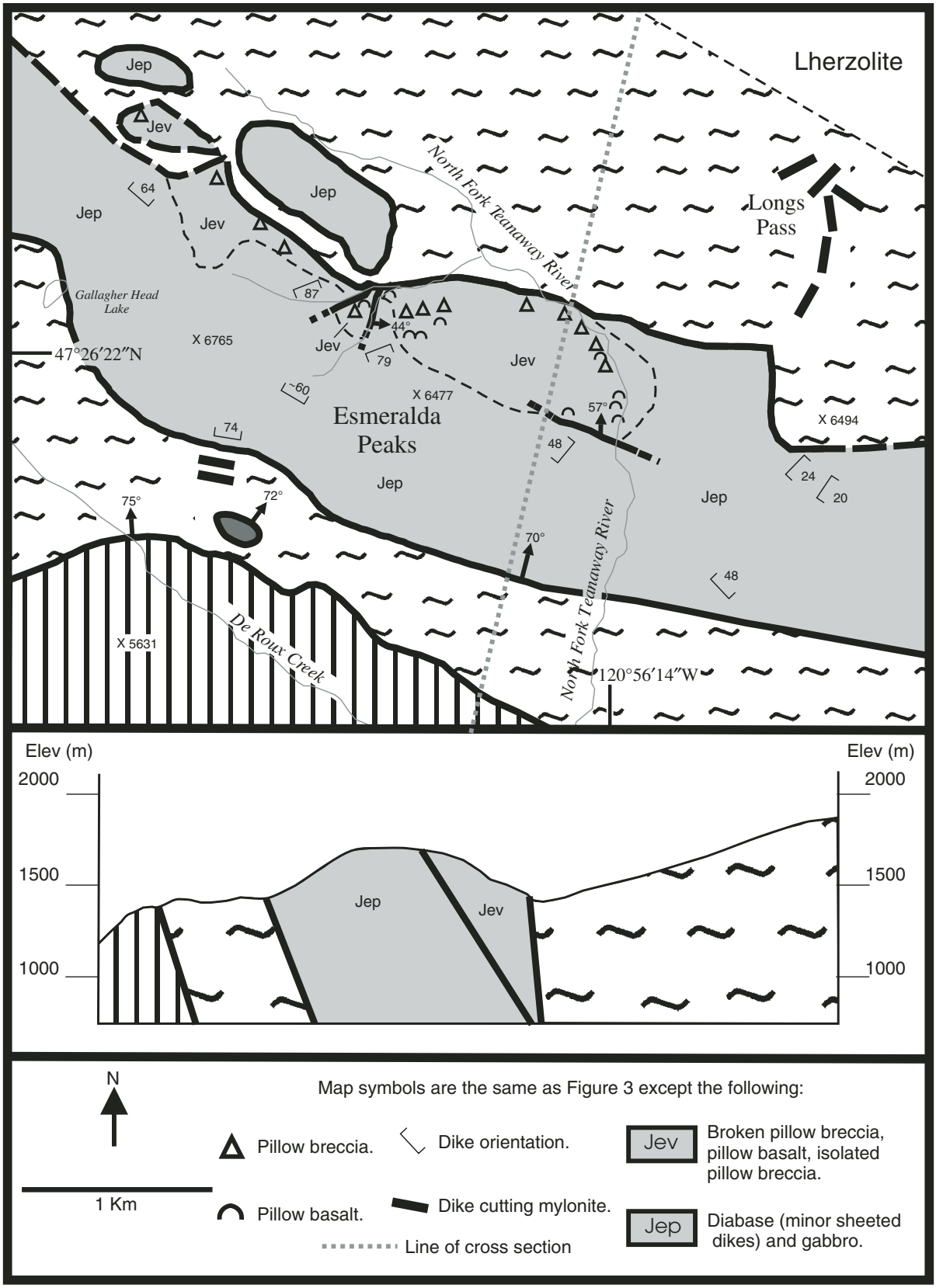

Figure 4. Geologic map of the Esmeralda Peaks and Longs Pass area of the Ingalls ophiolite complex. Mapping was done by MacDonald, R. Miller, and Harper. See Figure 3 for key and location.

podiform chromites, occurs south of the Navaho Divide fault zone (Fig. 3; Miller, 1980, 1985; Miller and Mogk, 1987). The northern lherzolite unit grades into the mylonitic lherzolite and hornblende peridotite that roughly coincide with the Navaho Divide fault zone; in contrast, the contact between the Navaho Divide fault zone and the southern harzburgite and dunite unit is a steep fault (Fig. 3; Miller, 1985; Miller and Mogk, 1987).

Mineral assemblages in the mylonitic peridotites record high temperatures (≥900 °C) that suggest they recrystallized in the mantle (Miller and Mogk, 1987). This observation and the spatial correspondence between the mylonites and serpentinite mélange led to the interpretation that the Navaho Divide fault zone is the shallow-level expression of this mantle shear zone (Miller, 1985; Miller and Mogk, 1987).

Ultramafic cumulates of wehrlite and clinopyroxenite occur in a >3-km-long, east-west–trending belt in the eastern part of the Ingalls ophiolite complex (Harper et al., 2003). The original relationship of these cumulates to the other ultramafic units is uncertain.

Mineralogy, textures, and Cr-spinel and whole-rock chemical compositions suggest that the northern lherzolite unit is the residue of mid-ocean-ridge basalt (MORB) magma extraction and display, or show, signs of referilization (Miller and Mogk, 1987; Metzger et al., 2002; Schultz et al., 2005). In contrast, the southern harzburgite underwent high degrees of partial melting, indicative of a suprasubduction-zone setting (Miller and Mogk, 1987; Metzger et al., 2002; Schultz et al., 2005). Cr-spinels in the southern dunites—which cut the harzburgites—have high Cr/(Cr + Al) ratios, which suggest that they formed when island-arc tholeiite- or boninitic-composition magmas passed through the harzburgite (Metzger et al., 2002).

The ultramafic tectonites vary from fresh peridotite to completely serpentinized. Serpentinites are commonly highly sheared. Diabase and gabbro dikes that cut the northern lherzolite and mylonitic peridotite are typically, but not invariably, altered to rodingite (Fig. 4), indicating intrusion prior to serpentinization (Miller, 1980; MacDonald et al., 2004). Miller (1985) described screens and xenoliths of mylonitic peridotites within gabbro. No mafic dikes have been observed to cut the southern harzburgite and dunite unit (Miller, 1980).

Iron Mountain Unit

The Iron Mountain unit consists of volcanic and minor sedimentary rocks, and it extends discontinuously for ~24 km in the southern portion of the complex (Fig. 3). This unit occurs as kilometer-scale and smaller fault-bounded blocks within the serpentinite mélange of the Navaho Divide fault zone (Figs. 3 and 4). Detailed petrology and geochemistry of the Iron Mountain unit can be found in MacDonald et al. (this volume, chapter 5).

Volcanic rocks within the Iron Mountain unit include vesicular basalt and broken pillow breccia, and minor rhyolite, basalt breccia, and hyaloclastite (Table 1) (MacDonald et al., this volume, chapter 5). Sedimentary rocks within the unit include argillite, chert, limestone, and very minor sandstone. Some of the limestone is oolitic and contains fossil fragments (MacDonald et al., 2002; Harper et al., 2003); none of these fossils provided ages (C.H. Stevens, 2002, written commun.).

Table 2 displays the major- and trace-element data for basalts and a rhyolite from the Iron Mountain unit. The basalts have geochemical affinities that are transitional between within-plate basalt and enriched mid-ocean-ridge basalt (E-MORB; Figs. 5, 6, and 7B). A rhyolite from the unit (Table 2) also has within-plate affinities; it appears to have been derived from the same mantle source as the basalts (Figs. 6 and 7B) and is interpreted to have formed by fractionation from the basaltic magmas.

A new U-Pb zircon date obtained from an Iron Mountain rhyolite (Fig. 3) has a weighted mean concordia age of 192.1 ± 0.3 Ma (mean square of weighted deviates [MSWD] of concordance = 3.3, including 2σ decay-constant errors) (MacDonald et al., this volume, chapter 5). Early Jurassic radiolarians, Pliensbachian and Upper Pliensbachian to Middle Toarcian, are reported

TABLE 1. REPRESENTATIVE PETROGRAPHY FROM INGALLS OPHIOLITE COMPLEX SAMPLES

Unit	Primary igneous minerals	Primary igneous textures	Predominate igneous crystallization sequence	Secondary alteration minerals
Esmeralda Peaks basalt	plagioclase; clinopyroxene; spinel; olivine†	subophitic; hyalophitic; microporphyry; vesicular†; variolitic†	clinopyroxene then plagioclase	albite; chlorite; epidote; pumpellyite; sphene
Esmeralda Peaks diabase	plagioclase; clinopyroxene; spinel	subophitic; microporphyry‡; ophitic†	clinopyroxene then plagioclase	albite; chlorite; epidote; pumpellyite; sphene; hornblende†; actinolite†
Esmeralda Peaks gabbro	plagioclase; clinopyroxene; spinel‡; hornblende†	hypidiomorphic-granular; poikilitic; ophitic‡; subophitic‡; pegmatitic†; cumulate†	clinopyroxene then plagioclase or hornblende then plagioclase	albite; chlorite; epidote; pumpellyite; sphene; hornblende‡; actinolite†
Esmeralda Peaks felsic plutonic	plagioclase; quartz; spinel‡; clinopyroxene†; hornblende†; K-feldspar†	hypidiomorphic-granular; microporphyry; felsophyric	plagioclase then quartz	albite; recrystallized quartz; sphene; chlorite‡; epidote‡; carbonate†
Iron Mountain basalt	spinel; plagioclase; clinopyroxene‡; olivine†	vesicular; microglomerophenocrysts; porphyry; microporphyry; vitrophyric; variolitic†	plagioclase then clinopyroxene	albite; chlorite; epidote; pumpellyite; sphene; carbonate
Iron Mountain rhyolite	quartz; plagioclase; spinel; muscovite†	porphyry; microporphyry; granular; felsophyric	plagioclase then quartz	albite; recrystallized quartz; epidote; sphene

†Rarely occurs in samples.
‡Occurs in some samples, but not all.

TABLE 2. ANALYSES OF IRON MOUNTAIN UNIT BASALT AND RHYOLITE SAMPLES

Sample:	BL-14–1[§§]	BL-95–1	BL-150	DRJM-16A	EL-42–2[§§]	IM-01A	IM-17	IM-32	IM-4	IM-40A	IM-70	IOE-77H
Rock type:	pillow basalt	pillow basalt	rhyolite	pillow basalt	pillow basalt	pillow basalt	pillow basalt	pillow basalt	pillow breccia	pillow basalt	pillow basalt	pillow basalt
Latitude:[†]	N47 24.126	N47 24.786	N47 25.090	N47 25.966	N47 25.631	N47 24.631	N47 24.711	N47 24.760	N47 24.910	N47 24.454	N47 24.949	N47 25.776
Longitude:	W120 38.677	W120 41.550	W120 44.005	W120 59.151	W120 51.401	W120 42.644	W120 42.812	W120 42.812	W120 43.444	W120 41.426	W120 44.665	W120 57.756
Magma type:[‡]	WPB	WPB	WPG	E-MORB	WPB	WPB	WPB	WPB	WPB	WPB	WPB	E-MORB
SiO_2	41.20	47.59	74.76	49.32	49.69	47.37	50.60	49.77	51.51	51.81	51.43	50.49
Al_2O_3	14.16	16.43	13.17	17.36	14.33	18.30	13.97	16.24	16.28	14.83	13.70	17.57
TiO_2	4.20	1.96	0.19	1.88	2.62	1.94	3.33	3.43	1.84	3.26	2.88	1.29
FeO^{T}[§]	11.05	8.84	2.94	11.50	12.15	12.21	13.00	11.53	9.69	11.68	13.59	11.18
MnO	0.20	0.17	0.03	0.17	0.20	0.14	0.18	0.12	0.15	0.12	0.21	0.19
MgO	2.91	6.42	0.12	2.48	4.37	3.29	3.94	2.13	6.61	3.53	5.78	6.86
CaO	21.69	14.49	0.71	9.74	9.90	12.41	10.23	10.28	8.64	8.55	7.27	6.98
Na_2O	2.85	3.65	4.86	4.20	5.74	3.91	4.10	4.68	4.78	4.80	4.44	4.71
K_2O	1.03	0.10	3.19	3.00	0.66	0.14	0.27	1.29	0.27	0.98	0.37	0.58
P_2O_5	0.72	0.35	0.04	0.36	0.34	0.30	0.38	0.53	0.23	0.43	0.33	0.14
Total[#]	100.00	100.00	100.00	100.00	100.00	100.00	100.00	100.00	100.00	100.00	100.00	100.00
LOI	N.D.[‡‡]	7.33	1.14	5.62	N.D.	5.34	3.87	6.45	4.99	3.09	2.86	4.15
Ba[††]	102	40	540	391	79	34	28	233	44	108	68	2108
Rb	29	3	46	76	14	3	8	48	2	30	7	8
Sr	246	128	46	305	264	187	150	232	152	195	135	271
Y	60	27	151	50	36	30	42	37	25	43	40	32
Zr	273	121	509	126	161	141	201	197	108	197	177	79
Nb	36.00	14.78	88.06	8.20	19.00	13.55	22.27	22.47	11.28	23.00	19.34	4.29
Th	2.08	2.16	10.05	N.D.	1.30	1.48	1.61	1.64	0.85	3.00	N.D.	0.29
Pb	N.D.	4.32	5.29	2.00	N.D.	1.45	1.02	1.21	N.D.	2.00	N.D.	0.23
Ga	N.D.	25	25	20	N.D.	26	19	20	16	20	19	17
Zn	164	99	121	155	157	77	130	169	80	144	117	92
Cu	23	118	2	53	57	45	106	49	86	57	113	54
Ni	15	69	12	147	31	39	38	37	50	34	26	171
V	331	246	11	256	303	277	357	294	230	314	345	287
Cr	8	232	0	366	46	123	58	125	198	59	36	366
Hf	7	N.D.	17	3	5	3	5	5	3	N.D.	N.D.	2
Cs	N.D.	N.D.	0.07	N.D.	N.D.	N.D.	N.D.	1.89	N.D.	N.D.	N.D.	0.66
Sc	28.00	32.38	2.20	40.00	34.00	36.60	37.00	31.60	34.10	32.00	43.31	43.40
Ta	2.12	N.D.	6.03	0.49	1.12	0.91	1.56	1.56	0.78	N.D.	N.D.	0.29
U	N.D.	N.D.	1.84	N.D.	N.D.	0.28	0.43	0.44	0.25	N.D.	N.D.	0.10
La	20.20	N.D.	74.70	8.73	11.80	13.49	16.35	15.22	9.11	9.00	23.16	4.52
Ce	55.20	17.27	150.17	19.32	30.80	26.99	36.69	32.74	20.01	53.00	38.27	10.63
Pr	N.D.	N.D.	18.26	2.78	N.D.	3.38	4.84	4.35	2.65	N.D.	N.D.	1.56
Nd	N.D.	N.D.	77.60	15.06	N.D.	15.87	23.12	20.75	12.73	N.D.	N.D.	8.41
Sm	8.28	N.D.	20.98	4.46	5.00	4.52	7.08	6.34	3.95	N.D.	N.D.	2.99
Eu	3.04	N.D.	3.51	1.54	1.84	1.62	2.39	2.31	1.44	N.D.	N.D.	1.20
Gd	N.D.	N.D.	22.06	5.86	N.D.	5.17	7.97	7.25	4.61	N.D.	N.D.	4.17
Tb	1.23	N.D.	4.14	1.08	N.D.	0.90	1.36	1.20	0.79	N.D.	N.D.	0.79
Dy	N.D.	N.D.	26.34	7.49	N.D.	5.58	8.20	7.22	4.83	N.D.	N.D.	5.46
Ho	N.D.	N.D.	5.48	1.66	N.D.	1.13	1.63	1.42	0.98	N.D.	N.D.	1.20
Er	N.D.	N.D.	15.28	4.81	N.D.	3.01	4.16	3.53	2.48	N.D.	N.D.	3.36
Tm	N.D.	N.D.	2.25	0.70	N.D.	0.43	0.57	0.49	0.33	N.D.	N.D.	0.49
Yb	4.88	N.D.	13.99	4.22	2.98	2.63	3.43	2.84	2.03	N.D.	N.D.	3.16
Lu	0.77	N.D.	2.13	0.60	0.49	0.41	0.52	0.42	0.31	N.D.	N.D.	0.50

[†]Lat/Long in hddd°mm.mmm' based on NAD27 CONUS datum.

[‡]Magma type determined using immobile trace-element discrimination diagrams. WPB—within-plate basalt; WPG—within-plate granite, E-MORB—enriched mid-ocean-ridge basalt.

[§]FeO^{T}—total iron as FeO.

[#]Normalized to 100% loss on ignition (LOI) free.

[††]If all trace elements are reported, analysis of Y, Zr, Cr, V, and Ni was by X-ray fluorescence (XRF); others are by inductively coupled plasma–mass spectrometry (ICP-MS). Otherwise, all analysis was done by XRF.

[‡‡]N.D.—no data.

[§§]Sample from Metzger et al. (2002).

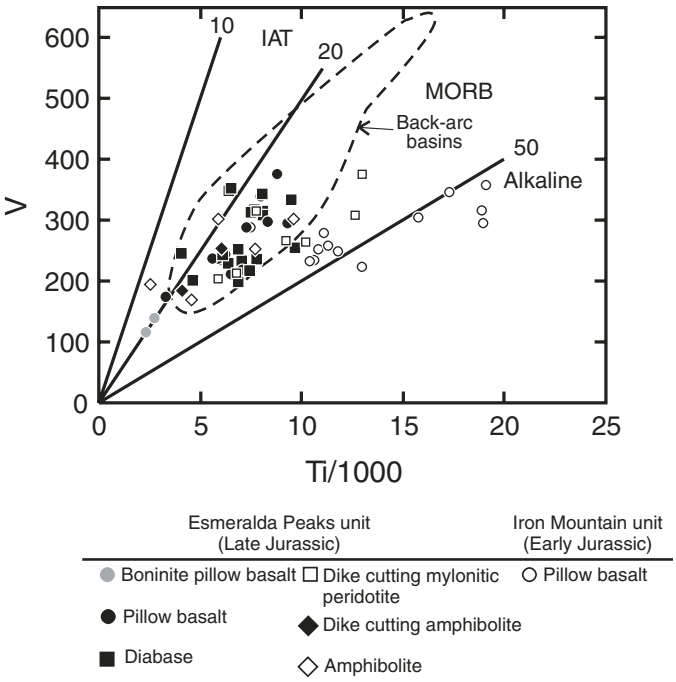

Figure 5. Ti-V basalt discrimination diagram (Shervais, 1982) displaying mafic rocks from the Ingalls ophiolite complex that have basaltic compositions. Gabbros are excluded because many of them appear to be cumulates. Field for back-arc basins was compiled by Metzger et al. (2002; references given in their Figure 6, p. 551) and Leat et al. (2000). IAT—island-arc tholeiite; MORB—mid-ocean-ridge basalt.

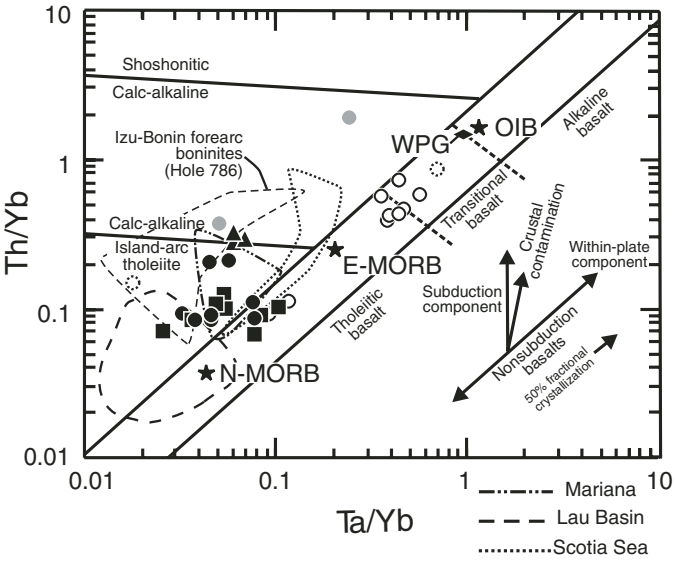

Figure 6. Th/Yb-Ta/Yb diagram from Pearce (1982) (Fig. 5 for key to symbols). Normal (N) mid-ocean-ridge basalt (MORB), enriched (E) MORB, and ocean-island basalt (OIB) normalizing values are from Sun and McDonough (1989). WPG—within-plate granite (from Harris, 1983). Fields for Mariana and Lau were compiled by Harper (2003a; their Fig. 7, p. 219), and Scotia Sea is from Leat et al. (2000). Field for Hole 786 boninites is from Murton et al. (1992).

from the Iron Mountain unit (Table 3; C. Blome, 1992, written commun.; E. Pessagno, 2004, written commun.). These Lower Jurassic radiolarian cherts occur within pillow basalts of the Iron Mountain unit or interbedded with argillites above the pillow basalts of the unit (MacDonald et al., this volume, chapter 5).

Esmeralda Peaks Unit

The Esmeralda Peaks unit was originally defined by Miller (1980, 1985) and is herein refined based on new field mapping, geochemistry, and U-Pb dating. This unit consists of kilometer-scale to smaller fault-bounded blocks of gabbro, diabase, basalt, and minor felsic and sedimentary rocks located within the serpentinite-matrix mélange of the Navaho Divide fault zone (Figs. 3 and 4). The faulted contacts of these blocks have an average strike of 269° and an average dip of 69°N (Fig. 4) (Miller, 1980, 1985). The Esmeralda Peaks unit extends the entire length of the complex (~30 km) and is internally faulted (Figs. 3 and 4). It ranges in thickness from <100 m to ~3 km, which is thinner than average oceanic crust (Miller, 1980, 1985). Although the blocks that make up the Esmeralda Peaks units are part of a mélange, some are sufficiently large that they enclose an intact ophiolite "stratigraphy" within them.

Lithologies

Gabbro is a minor component of the Esmeralda Peaks unit. It ranges from fine-grained to pegmatitic (Table 1), and it is complexly intermingled with diabase or cut by diabase dikes, which range from 10 to 50 cm in thickness. The gabbro displays weak magmatic foliation and local cumulate textures (Table 1).

Fine-grained tonalite and trondhjemite dikes occur locally within the Esmeralda Peaks unit (Table 1). These felsic dikes commonly cut gabbro and diabase and are locally cut by diabase dikes (Miller, 1980).

Diabase is the most common rock type within the Esmeralda Peaks unit (Fig. 4). It is massive or occurs as dikes. Diabase dikes are up to ~1 m in thickness, vary in strike, and have moderate to steep dips; true sheeted dikes are rare (Fig. 4) (Miller, 1980, 1985). Due to the extensive faulting, original orientations of the dikes are not known. Diabase dikes also cut and, in rare cases, feed into pillow basalts and broken pillow breccias (Miller, 1980; Metzger et al., 2002).

Figure 7. Chondrite- and normal (N) mid-ocean-ridge basalt (MORB)–normalized diagrams (see Fig. 5 for key to symbols). Chondrite and N-MORB normalized values are from Sun and McDonough (1989). Gabbros are not plotted due to their apparent cumulate geochemical affinities. (A) Modern reference suite. Ocean-island granite (OIG) and within-plate granite (WPG) are from Harris (1983); N-MORB, enriched (E) MORB, and ocean-island basalt (OIB) are from Sun and McDonough (1989); island-arc tholeiite (IAT) is from Pearce et al. (1995); boninite is from Pearce and Parkinson (1993). (B) Iron Mountain unit basalts and rhyolite. (C) Esmeralda Peaks unit basalts and diabase. (D) Esmeralda Peaks unit felsic plutonic rocks (triangles) and boninites.

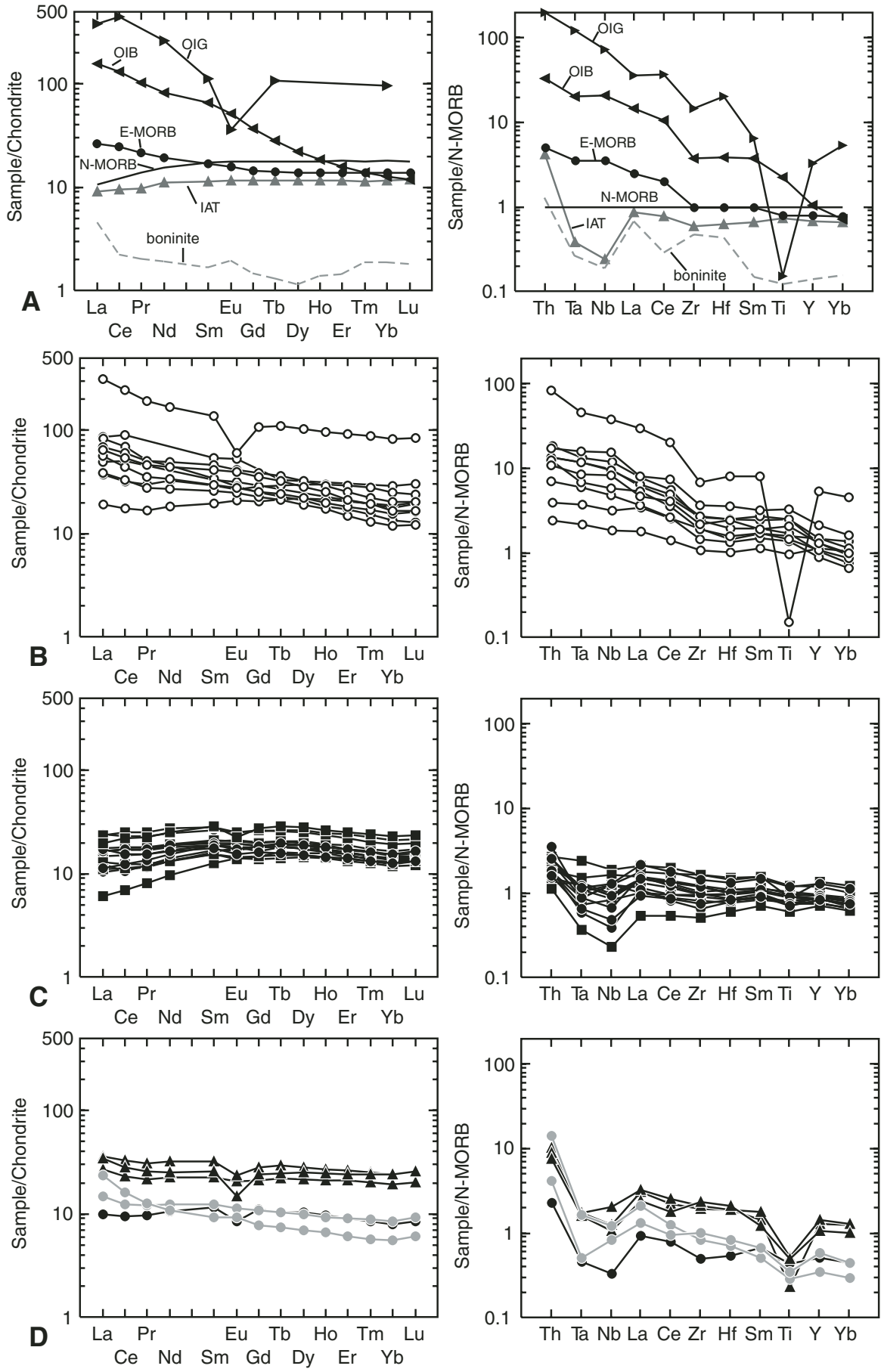
A
B
C
D
Sample/Chondrite
Sample/N-MORB
OIG
OIB
E-MORB
N-MORB
IAT
boninite
La Ce Pr Nd Sm Eu Gd Tb Dy Ho Er Tm Yb Lu
Th Ta Nb La Ce Zr Hf Sm Ti Y Yb
500
100
10
1
0.1

TABLE 3. JURASSIC RADIOLARIAN AGES FROM THE INGALLS OPHIOLITE COMPLEX

Sample no.	Latitude (°N)	Longitude (°W)	Age	Radiolaria
BL-21–1†	47°24′12.5″	120°38′53.2″	Early Jurassic (Pliensbachian undifferentiated)	*Canoptum* sp. ?, *Noritus* sp., *Praeconocaryomma* sp., *Zartus mostleri*
BL-22–1†	47°24′10.0″	120°38′55.2″	Probably Early Jurassic (Pliensbachian ?)	*Canoptum* sp. ?, *Praeconocaryomma* sp., *Praeconocaryomma immodica*
BL-48–1†	47°24′27.5″	120°41′00.0″	Early Jurassic (probably late Pliensbachian)	*Canoptum* sp. Aff. *C. rugosum, Canutus haimaensis, Canutus izeensis, Hsuum mulleri, Praeconocaryomma parvimamma, Protopsium* sp., *Trillus elkhornensis, Zartus* sp. Aff. *Z. mostleri*
IM-74E‡	47°25′03.0″	120°44′34.5″	Upper Pliensbachian to middle Toarcian	*Paracanoptum annulatum, Parahsuum* sp.
IGH-70e‡	47°24′18.9″	120°38′33.6″	Uppermost Callovian? to lower Oxfordian	*Praecameta decora, Hsuum brevicostatum, Spongocapsula palmerae, Archaeodictyomitra* n. sp., *Pantanellium* sp., *Gorgansium* sp., *Praeconocaryomma immodica*
BL-73–1‡	47°24′55.74″	120°40′55.53″	Lower Oxfordian	*Pachyoncus kamiasonens, Pantanellium darlingtonense, Pantanellium* sp., *Ristola procera*
IM-70E‡	47°24′18.9″	120°38′33.6″	Lower Oxfordian	*Linaresia beniderkalensis, Hsuum brevicostata, Pantanellium darlingtonense, Pantanellium* sp., *Gorgansium* sp.
EL-92–4‡	47°24.70	120°47.58	Upper Callovian to lower middle Oxfordian	*Hsuum brevicostatum*
FC-13–1†	47°24.17′	120°38.49′	Probably Late Jurassic	*Archaeodictyomitra apiara, Archaeodictyomitra* sp., *Katroma* sp. ?, *Lithocampe* sp. ?, *Mirifusus* sp. ?, Unidentifiable pantanelliids
FC-14–2†	47°24.25′	120°38.44′	Late Jurassic (probably Oxfordian or Kimmeridgian)	*Higumastra* sp., *Parvicingula* sp., *Praeconocaryomma* sp., *Hsuum maxwelli* group

†Fossil and age determinations made by C.D. Blome (1992).
‡Fossil and age determinations made by E.A. Pessagno Jr. (1999–2004).

Pillow basalts are common within the Esmeralda Peaks unit (Fig. 4). Pillows are typically lobate, range up to ~1 m in diameter, and have <1-cm-wide, fine-grained rims that are altered to chlorite. Broken pillow breccia is widespread throughout the extrusive rocks (Fig. 4). Angular clasts within broken pillow breccia are a few centimeters in diameter and are supported by a matrix of red or green chert that contains recrystallized radiolarians. Chert-supported isolated pillow breccia, consisting of lobate pillows 6–25 cm in diameter, occurs locally.

Minor sedimentary rocks are intercalated with the pillow basalts. These include red and green chert and rare ophiolitic breccia. The ophiolitic breccia consists of angular centimeter-size clasts of predominantly basalt and diabase, with lesser gabbro and rare felsic clasts. Red and green chert makes up the matrix of the breccia.

Petrography

A brief outline of the petrography of the Esmeralda Peaks unit is given here. Detailed petrography of the Esmeralda Peaks unit can be found in Miller (1980), MacDonald (2006), and Table 1. Gabbros commonly display hypidiomorphic-granular textures, but other textures exist (see Table 1). Relict plagioclases (~An_{70} to An_{75}; based on extinction angles) are not zoned and commonly show albite twins. Felsic plutonic samples have predominantly hypidiomorphic-granular igneous textures (Table1).

Diabases are subophitic, and there are a few transitional to ophitic textures (Table 1). Basalts range from subophitic to hyalophitic, and microphenocrysts of clinopyroxene are common (Table 1). Rims of Esmeralda Peaks basalts typically have <1% vesicles, suggesting that they erupted in deep water (Moore, 1970), or they have a low primary H_2O. Several basalts have highly vesicular rims and variolitic textures (Table 1), typical of boninites (e.g., Cameron et al., 1980; Harper, 2003a).

The common alteration minerals in the Esmeralda Peaks unit indicate prehnite-pumpellyite to lower greenschist-facies metamorphism (Table 1). Esmeralda Peaks gabbro and some of the diabase show higher-grade, amphibolite-facies alteration (Table 1). This higher-temperature metamorphism is typical of the deeper levels of altered oceanic crust (e.g., Mottl, 1983; Seyfried, 1987). The hornblendes in these gabbros and diabases have been overprinted by greenschist-facies minerals, suggesting a retrograde metamorphic progression.

Geochemistry

A large geochemical database (n = 106) now exists for the Ingalls ophiolite complex (see GSA Data Repository[1] for analytical discussion) (Gray, 1982; Ort and Tabor, 1985; Metzger et al., 2002; this chapter). However, data for most samples from previous studies (n = 54) are of limited use due to several critical aspects: (1) there are no reported localities for some samples;

[1]GSA Data Repository Item 2008065, Analytical methods, is available on request from Documents Secretary, GSA, P.O. Box 9140, Boulder, CO 80301-9140, USA, or editing@geosociety.org, at www.geosociety.org/pubs/ft2008.htm.

(2) element contamination occurred during processing for a number of samples; and (3) all but Gray's (1982) samples were collected during reconnaissance-level field mapping (which is unsuitable due to the complex nature of the geology; see Metzger et al. [2002] for discussion). The samples of Metzger et al. (2002) were analyzed at the same laboratory as our samples (Washington State University GeoAnalytical Laboratory), eliminating possible interlaboratory comparison concerns. Therefore, greatest emphasis is placed on the data of Metzger et al. (2002), as well as our new analyses, and only nine samples combined from Gray (1982) and Ort and Tabor (1985) are used in this paper and plotted on the geochemical diagrams that follow.

Volcanic and plutonic rocks of the Iron Mountain and Esmeralda Peaks units have undergone greenschist-facies metamorphism (Table 1; Fig. 2). A number of important geochemical elements are mobile under greenschist-facies conditions (Cann, 1970; Harper et al., 1988; Harper, 1995). However, several key elements that give insights into igneous petrogenesis (Ti, V, Th, Cr, Ta, Hf, Y, and rare earth elements [REEs]) generally remain immobile up to and including amphibolite-facies metamorphic conditions (Pearce, 1996a). Therefore, only these immobile elements are used on geochemical diagrams in this paper.

Table 4 displays whole-rock major- and trace-element data for basalt, diabase, and felsic plutonic samples from the Esmeralda Peaks unit. Gabbros from the Esmeralda Peaks unit are given in Table 5 but are not plotted on most geochemical diagrams because of their excess in the elements Cr, Sc, Al, and Ni (Table 5). These elemental excesses suggest that they do not represent a "true" melt composition (Pearce, 1996a), although the gabbros generally do not have cumulate textures.

The pillows, pillow breccias, and diabases range in composition from basalts through andesites (Table 4). Ti/V, Cr/Y, Cr/Yb, Th/Yb-Ta/Yb, chondrite- and MORB-normalized diagrams indicate magmatic affinities that are island-arc tholeiite (IAT), MORB, and transitional between IAT and MORB (Figs. 5, 6, 7C, and 8) (Shervais, 1982; Pearce, 1982; Pearce and Parkinson, 1993). Ta/Yb ratios, Y and Yb values, and MORB-normalized patterns suggest that these rocks originated from a mantle that was slightly enriched from normal (N) MORB and that underwent a high degree of melting (Figs. 6, 7C, and 8) (Pearce, 1982; Sun and McDonough, 1989; Pearce and Peate, 1995; McDonough and Sun, 1995). They are generally enriched in Th and depleted in Ta and Nb with respect to N-MORB (Fig. 7C), which are characteristics of magmas erupted in suprasubduction-zone settings (e.g., Pearce et al., 1984).

The felsic plutonic rocks from the Esmeralda Peaks unit (Table 4) have chondrite- and MORB-normalized patterns that are similar to, but elevated from, the pillows, pillow breccias, and diabases of the unit (Figs. 7C and 7D). They have negative Eu and Ti anomalies (Fig. 7D), which suggest extensive plagioclase and Fe-Ti–oxide fractionation. These felsic plutonic samples plot transitionally between IAT and calc-alkaline basalts (CAB) on the Th/Yb versus Ta/Yb diagram (Fig. 6).

Two variolitic pillow basalt samples from the Esmeralda Peaks unit have SiO_2, TiO_2, and MgO values that classify them as boninites (EL-72-3 and IO-111; Table 4; Le Maitre, 2002). A third variolitic pillow basalt from the Esmeralda Peaks unit, which does not have SiO_2 and MgO values of a boninite (MS-15B; Table 4), was classified as a boninite by Metzger et al. (2002) based on petrographic criteria of Cameron et al. (1980) and other geochemical criteria. We agree with this interpretation. These three samples have elevated Cr and are depleted in Y and Yb with respect to other Esmeralda Peaks samples (Fig. 8). They have chondrite- and N-MORB–normalized values that are generally lower than other Esmeralda Peaks samples, and one sample has a typically boninitic "u-shaped" chondrite-normalized pattern (EL-72-3; Fig. 7D) (Beccaluva and Serri, 1988). When normalized to fertile MORB mantle, the patterns for these three samples (Fig. 9A) are enriched in the moderately and highly compatible elements Cr, Mg, and Ni. They are depleted in the moderately and highly incompatible elements Sc, V, Yb, Y, and Ti with respect to other Esmeralda Peaks samples (Fig. 9A). Due to the hydrothermal greenschist-facies alteration of these samples, which mobilizes Ca (Seyfried, 1987; Harper et al., 1988; Berndt et al., 1988; Harper, 1995), it is not possible to use the high- versus low-Ca boninite classification of Crawford et al. (1989); however, the pyroxene phenocrysts in these samples are augite (determined optically), which is common in high-Ca boninites (Crawford et al., 1989).

Geochronology

Miller et al. (2003) reported a new U-Pb zircon date from a hornblende pegmatite gabbro of the Esmeralda Peaks unit (161 ± 1 Ma; 2σ weighted mean $^{206}Pb/^{238}U$ age of three nearly concordant fractions) (Fig. 3). This date is significantly older than a previous, apparently discordant, U-Pb zircon age (155 ± 2 Ma) (Hopson and Mattinson, 1973; Miller et al., 1993) for a gabbro from the same general sample locality as Miller et al.'s (2003) sample (C. Hopson, 2005, personal commun.).

Amphibolite and Dikes

Amphibolite occurs in the western portion of the Ingalls ophiolite complex as a fault-bounded block within the Navaho Divide fault zone (Fig. 3) and in the Cle Elum Ridge fault zone (Frost, 1973, 1975; Miller, 1980, 1985). Amphibolites in the roof pendant of the Mount Stuart batholith (Fig. 2) are the result of Cretaceous metamorphism and are not directly related to the other amphibolites of the Ingalls ophiolite complex (Miller, 1980, 1985, 1988). The amphibolites tend to be massive and display well-preserved igneous textures (Fig. 10A), or they are strongly foliated to mylonitic (Fig. 10B). They are mostly derived from gabbro and, less commonly, from diabase and basalt. Some of the amphibolites are commonly cut by undeformed diabase dikes (Fig. 10), suggesting that metamorphism and deformation occurred during subseafloor metamorphism.

The amphibolites and dikes that cut them (Table 6) have similar Ti/V, Cr/Y, and Cr/Yb ratios as the Esmeralda Peaks samples (Figs. 5 and 8) (Metzger et al., 2002). The dikes have similar fertile MORB mantle–normalized patterns as the Esmeralda Peaks unit

TABLE 4. ANALYSES OF ESMERALDA PEAKS UNIT BASALT, DIABASE, AND FELSIC PLUTONIC SAMPLES

Sample:	BL-112-1	EL-72-3	EL-77-1	IOE-18	IOE-41D	IOE-48D	IOE-49	IOE-TOP	BL-72[§§]	BL-75-1[§§]
Rock type:	pillow basalt	pillow basalt	pillow breccia	pillow basalt	diabase dike	diabase dike	diabase	diabase	diabase	pillow basalt
Latitude:[†]	N47 28.350	N47 25.565	N47 25.595	N47 26.365	N47 25.937	N47 26.746	N47 26.462	N 47 26.231	N47 24.923	N47 24.845
Longitude:	W120 39.816	W120 45.969	W120 46.168	W120 56.227	W120 57.174	W120 58.217	W120 58.548	W120 57.417	W120 40.543	W120 40.973
Magma type:[‡]	IAT-MORB	BON	MORB	IAT-MORB	IAT	IAT	MORB	MORB	IAT	IAT
SiO_2	53.76	56.45	56.11	54.09	57.27	56.51	53.84	53.38	48.19	53.98
Al_2O_3	15.51	13.8	17.05	17.51	15.48	16.01	15.43	15.97	16.00	16.67
TiO_2	1.55	0.38	1.08	1.26	1.02	1.07	1.30	1.19	0.80	1.01
FeO^{T}[§]	10.26	5.71	5.80	9.63	7.47	7.52	8.67	9.26	7.96	9.78
MnO	0.17	0.15	0.23	0.12	0.16	0.14	0.16	0.20	0.14	0.13
MgO	4.93	8.41	5.41	7.78	5.91	6.54	6.03	7.19	8.93	5.49
CaO	8.14	11.68	7.65	4.85	6.68	6.33	9.82	8.13	16.45	7.24
Na_2O	5.08	2.79	5.23	4.50	5.77	5.59	4.42	3.92	1.19	5.46
K_2O	0.44	0.58	1.29	0.14	0.15	0.18	0.21	0.64	0.29	0.13
P_2O_5	0.16	0.05	0.16	0.13	0.11	0.11	0.14	0.13	0.06	0.10
Total[#]	100.00	100.00	100.00	100.00	100.00	100.00	100.00	100.00	100.00	100.00
LOI	3.93	4.68	2.34	3.83	1.57	2.43	1.82	2.4	2.22	2.91
Ba[††]	58	130	435	27	49	18	29	48	531	72
Rb	8	11	25	2	1	1	5	6	4	3
Sr	210	414	369	110	185	59	131	304	400	178
Y	37	10	25	27	22	25	27	24	20	26
Zr	110	64	90	74	63	70	93	92	39	50
Nb	3.00	2.94	3.00	3.00	2.00	3.00	4.00	2.36	0.56	0.94
Th	0.32	1.76	N.D.[‡‡]	0.22	0.22	0.28	0.23	0.16	0.14	0.23
Pb	0.76	5.10	N.D.	0.77	0.27	0.21	0.38	0.32	N.D.	N.D.
Ga	15	14	12	17	11	14	11	14	N.D.	N.D.
Zn	79	54	54	78	32	30	72	31	62	84
Cu	67	53	29	71	23	4	13	163	76	27
Ni	44	257	32	40	26	33	30	48	104	41
V	296	117	213	315	244	230	239	253	203	239
Cr	137	461	140	20	34	32	64	135	301	210
Hf	2.81	1.49	N.D.	2.04	1.64	1.77	2.34	2.11	1.29	1.67
Cs	0.58	0.50	N.D.	0.18	0.03	0.30	1.85	0.54	N.D.	N.D.
Sc	40.20	23.33	34.00	38.00	34.00	41.00	38.00	38.60	37.80	40.60
Ta	0.16	0.22	N.D.	0.12	0.10	0.12	0.21	0.18	0.05	0.08
U	0.07	0.36	N.D.	0.16	0.09	0.15	0.09	0.09	N.D.	N.D.
La	5.59	5.49	7.00	2.63	2.60	3.03	4.09	3.84	1.40	2.86
Ce	13.89	9.61	22.00	7.42	6.87	7.43	10.87	10.28	4.18	6.38
Pr	2.13	1.17	N.D.	1.26	1.11	1.15	1.67	1.59	0.75	1.14
Nd	11.26	5.01	N.D.	7.16	6.02	6.23	8.82	8.28	4.46	6.46
Sm	3.97	1.39	N.D.	2.84	2.30	2.31	3.17	2.85	1.91	2.54
Eu	1.43	0.53	N.D.	0.98	0.78	0.82	1.18	1.03	0.80	0.96
Gd	5.17	1.57	N.D.	3.70	3.01	2.99	3.96	3.64	2.79	3.65
Tb	0.97	0.27	N.D.	0.72	0.56	0.59	0.75	0.67	0.52	0.69
Dy	6.52	1.73	N.D.	4.70	3.76	3.94	4.91	4.38	3.63	4.72
Ho	1.38	0.37	N.D.	1.01	0.81	0.87	1.04	0.93	0.78	1.02
Er	3.88	0.98	N.D.	2.78	2.26	2.37	2.83	2.59	2.15	2.77
Tm	0.56	0.14	N.D.	0.40	0.33	0.36	0.41	0.37	0.32	0.40
Yb	3.52	0.93	N.D.	2.60	2.05	2.26	2.51	2.35	1.96	2.46
Lu	0.54	0.15	N.D.	0.41	0.33	0.35	0.39	0.36	0.30	0.37

(*continued.*)

TABLE 4. ANALYSES OF ESMERALDA PEAKS UNIT BASALT, DIABASE, AND FELSIC PLUTONIC SAMPLES (*continued.*)

Sample:	EL-79-1	EL-79-2	EL-92-1	IO-111	IO-136	IO-15	MS-42-1	MS-14-2	IOE-47
Rock type:	diabase dike	pillow basalt	pillow breccia	pillow basalt	diabase	pillow basalt	tonalite dike	tonalite	trondhjemite
Latitude:†	N47 25.515	N47 25.515	N47 24.701	N47 25.735	N47 25.941	N47 25.565	N47 26.748	N47 25.584	N47 26.551
Longitude:	W120 46.179	W120 46.179	W120 47.577	W120 41.286	W120 41.371	W120 38.437	W120 57.450	W120 53.532	W120 58.099
Magma type:‡	IAT-MORB	MORB	IAT	BON	IAT-MORB	MORB	VAG	VAG	VAG
SiO_2	51.76	54.53	56.36	59.94	58.98	52.51	68.28	69.54	76.78
Al_2O_3	18.04	16.71	15.68	13.28	15.07	16.20	15.12	14.93	12.17
TiO_2	1.25	1.18	0.99	0.46	1.15	1.39	0.69	0.66	0.31
FeO^{T}§	6.91	7.30	7.28	5.95	8.38	8.92	3.01	4.13	2.22
MnO	0.16	0.15	0.10	0.14	0.16	0.18	0.03	0.04	0.01
MgO	4.84	5.30	4.21	9.41	4.89	4.74	1.90	1.90	0.68
CaO	11.68	9.47	9.91	7.26	6.07	11.36	4.62	1.69	2.48
Na_2O	4.35	5.18	5.28	3.25	4.90	4.51	5.90	6.74	5.18
K_2O	0.86	0.05	0.05	0.24	0.26	0.06	0.24	0.20	0.09
P_2O_5	0.16	0.14	0.14	0.08	0.14	0.13	0.22	0.17	0.09
Total#	100.00	100.00	100.00	100.00	100.00	100.00	100.00	100.00	100.00
LOI	4.87	2.77	6.06	6.58	1.65	4.5	2.36	1.77	0.94
Ba††	131	15	28	60	48	34	36	31	17
Rb	25	1	0	6	8	2	3	2	1
Sr	255	63	87	141	106	81	160	67	83
Y	26	25	22	17	39	33	42	31	38
Zr	98	91	75	78	126	86	161	181	147
Nb	3.60	2.27	1.64	2.00	3.00	2.50	5.00	2.60	3.01
Th	2.00	0.19	0.44	0.52	0.32	N.D.	1.10	0.94	1.28
Pb	1.00	0.88	0.74	0.63	1.00	N.D.	0.56	0.47	0.85
Ga	18	17	19	10	14	17	14	13	11
Zn	67	56	60	56	79	72	7	13	1
Cu	38	33	170	13	49	67	6	4	6
Ni	19	66	34	143	57	48	6	12	11
V	219	220	236	141	201	299	46	91	43
Cr	47	41	41	489	133	122	4	7	0
Hf	N.D.	2.15	1.84	1.79	3.04	N.D.	3.96	4.45	3.97
Cs	N.D.	0.05	0.21	0.24	0.28	N.D.	0.11	0.14	0.06
Sc	31.99	35.67	32.44	30.70	32.60	34.00	15.00	15.30	13.60
Ta	N.D.	0.17	0. 12	0.07	0.14	N.D.	0.24	0.22	0.24
U	N.D.	0.43	0.22	0.18	0.12	N.D.	0.38	0.26	0.45
La	†	3.86	4.01	3.40	4.63	2.00	8.46	6.21	8.05
Ce	30.99	10.46	9.37	7.47	13.12	23.00	19.95	13.92	17.11
Pr	N.D.	1.61	1.45	1.12	2.09	N.D.	2.89	2.00	2.39
Nd	N.D.	8.71	7.55	5.65	11.46	N.D.	14.78	10.27	11.64
Sm	N.D.	2.98	2.64	1.84	4.28	N.D.	4.84	3.35	3.88
Eu	N.D.	1.13	0.88	0.64	1.28	N.D.	1.34	1.18	0.84
Gd	N.D.	3.77	3.23	2.16	5.56	N.D.	5.71	4.23	4.82
Tb	N.D.	0.67	0.59	0.38	1.05	N.D.	1.07	0.81	0.91
Dy	N.D.	4.35	3.74	2.48	7.03	N.D.	6.97	5.41	6.24
Ho	N.D.	0.89	0.81	0.51	1.48	N.D.	1.50	1.16	1.37
Er	N.D.	2.50	2.27	1.47	4.12	N.D.	4.28	3.40	3.93
Tm	N.D.	0.34	0.33	0.22	0.61	N.D.	0.63	0.50	0.60
Yb	N.D.	2.15	2.09	1.40	3.83	N.D.	4.02	3.21	4.00
Lu	N.D.	0.34	0.33	0.23	0.59	N.D.	0.64	0.50	0.64

†Lat/Long in hddd°mm.mmm' based on NAD27 CONUS datum.

‡Magma type determined using immobile trace-element discrimination diagrams. MORB—mid-ocean-ridge basalt, IAT—island-arc tholeiite, IAT-MORB—transitional island-arc tholeiite–mid-ocean-ridge basalt, VAG—transitional volcanic-arc granite.

§FeO^{T}—total iron as FeO.

#Normalized to 100% loss on ignition (LOI) free.

††If all trace elements are reported, analysis of Y, Zr, Cr, V, and Ni was by X-ray fluorescence (XRF); others are by inductively coupled plasma–mass spectrometry (ICP-MS). Otherwise, all analysis was done by XRF.

‡‡N.D.—no data.

§§Sample from Metzger et al. (2002).

TABLE 5. SELECTED ANALYSES OF ESMERALDA PEAKS UNIT GABBROS

Sample:	BL-137–1	BL-90–2	EL-87–2	EL-49B	IC-14G	IC-17A	MS-26–2	IOE-41G[§§]	IOE-48G[##]	MS-38–1
Rock type:	gabbro pegmatite	gabbro	gabbro	gabbro cumulate	gabbro	gabbro	gabbro	gabbro	gabbro	gabbro
Latitude:[†]	N47 27.423	N47 25.182	N47 25.229	N 47 25.622	N47 27.323	N47 27.194	N47 25.752	N47 25.937	N47 26.746	N47 25.902
Longitude:	W120 41.404	W120 39.516	W120 47.993	W120 51.991	W120 41.643	W120 41.707	W120 58.902	W120 57.174	W120 58.217	W120 53.616
Magma type:[‡]	IAT-MORB	IAT	MORB	IAT	IAT	IAT	IAT	IAT	IAT	MORB
SiO_2	53.45	46.41	50.76	51.27	54.27	48.46	51.69	51.57	54.19	48.65
Al_2O_3	18.58	23.15	17.03	19.39	17.35	22.61	14.40	16.31	18.72	16.38
TiO_2	0.56	0.12	0.48	0.21	0.29	0.15	0.35	0.11	0.48	0.98
$FeO^{T§}$	5.03	4.36	5.35	4.25	4.73	3.76	5.28	6.40	6.03	8.14
MnO	0.10	0.07	0.11	0.09	0.13	0.07	0.14	0.14	0.12	0.15
MgO	5.52	13.14	10.69	8.09	7.48	7.02	10.25	13.14	6.69	9.09
CaO	12.10	10.83	12.82	13.65	12.35	15.51	15.27	8.59	8.95	13.58
Na_2O	4.29	1.81	2.49	2.98	3.29	2.28	2.59	1.51	4.62	2.85
K_2O	0.31	0.10	0.24	0.06	0.08	0.13	0.03	2.21	0.16	0.11
P_2O_5	0.06	0.02	0.03	0.01	0.03	0.02	0.01	0.01	0.05	0.06
Total[#]	100.00	100.00	100.00	100.00	100.00	100.00	100.00	100.00	100.00	100.00
LOI	2.17	5.16	2.38	2.33	0.63	2.43	2.18	3.54	3.33	2.50
Ba[††]	29	3	23	25	90	18	4	438	18	39
Rb	5	1	3	1	1	2	1	20	1	1
Sr	191	176	128	204	180	203	84	188	109	320
Y	17	3	13	7	8	4	12	4	15	22
Zr	40	13	23	10	19	11	12	10	43	35
Nb	0.56	0.09	0.20	1.00	0.33	0.09	0.07	0.10	0.75	0.75
Th	0.06	0.04	0.02	1.00	0.15	0.05	0.04	0.04	0.37	0.03
Pb	0.43	0.13	0.18	N.D.[‡‡]	1.33	0.18	0.17	0.14	0.39	0.38
Ga	15	13	13	13	12	12	9	8	16	15
Zn	30	27	32	21	80	21	30	35	33	48
Cu	21	64	83	68	4	62	79	65	7	62
Ni	48	427	189	99	104	156	114	228	60	109
V	156	19	168	110	124	56	187	135	191	248
Cr	193	883	900	497	950	364	583	493	125	394
Hf	1.06	0.17	0.55	N.D.	0.43	0.15	0.31	0.14	1.16	1.02
Cs	0.57	0.11	0.03	N.D.	0.07	0.36	0.03	0.24	0.29	0.09
Sc	33.00	3.90	42.27	21.00	36.80	15.21	57.20	38.40	36.10	44.10
Ta	0.04	0.01	0.02	N.D.	0.03	0.01	0.01	0.01	0.07	0.06
U	0.01	0.01	0.01	N.D.	0.08	0.01	0.01	0.02	0.17	0.01
La	1.77	0.33	0.55	N.D.	1.09	0.38	0.42	0.38	2.26	1.06
Ce	4.05	0.77	1.97	N.D.	2.43	1.00	1.08	0.73	5.1	3.44
Pr	0.68	0.13	0.36	N.D.	0.37	0.16	0.22	0.11	0.75	0.66
Nd	3.98	0.69	2.36	N.D.	1.95	0.85	1.53	0.56	3.83	4.21
Sm	1.62	0.28	1.08	N.D.	0.78	0.35	0.85	0.24	1.42	1.95
Eu	0.91	0.18	0.51	N.D.	0.41	0.33	0.54	0.15	0.61	0.81
Gd	2.27	0.38	1.64	N.D.	1.08	0.48	1.44	0.41	1.96	2.86
Tb	0.44	0.07	0.33	N.D.	0.21	0.09	0.3	0.08	0.38	0.59
Dy	2.97	0.49	2.23	N.D.	1.4	0.64	2.11	0.59	2.52	3.99
Ho	0.64	0.1	0.49	N.D.	0.31	0.13	0.46	0.14	0.58	0.85
Er	1.79	0.31	1.36	N.D.	0.81	0.39	1.26	0.41	1.59	2.39
Tm	0.25	0.04	0.20	N.D.	0.12	0.06	0.18	0.06	0.25	0.34
Yb	1.59	0.27	1.21	N.D.	0.73	0.33	1.12	0.41	1.55	2.09
Lu	0.25	0.04	0.18	N.D.	0.11	0.05	0.17	0.07	0.26	0.32

[†]Lat/Long in hddd°mm.mmm' based on NAD27 CONUS datum.

[‡]Magma type determined using immobile trace-element discrimination diagrams. MORB—mid-ocean-ridge basalt, IAT—island-arc tholeiite, IAT-MORB—transitional island-arc tholeiite–mid-ocean-ridge basalt.

[§]FeO^T—total iron as FeO.

[#]Normalized to 100% loss on ignition (LOI) free.

[††]If all trace elements are reported, analysis of Y, Zr, Cr, V, and Ni was by X-ray fluorescence (XRF); others are by inductively coupled plasma–mass spectrometry (ICP-MS). Otherwise, all analysis was done by XRF.

[‡‡]N.D.—no data.

[§§]Is cut by sample IOE-41D.

[##]Is cut by sample IOE-48D.

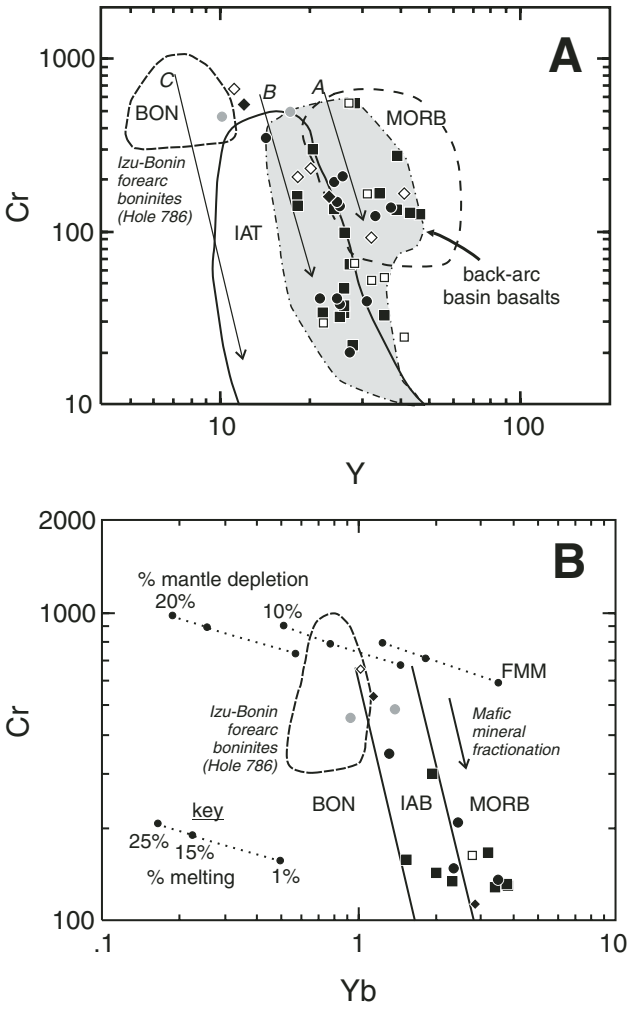

Figure 8. (A) Cr-Y discrimination diagram (Pearce, 1982) (see Figure 5 for key to symbols). Arrows A, B, and C represent crystallization paths for magmas fractionating Cr-spinel + olivine + pyroxene for mid-ocean-ridge basalt (MORB), island-arc tholeiite (IAT), and boninites (BON) respectively. See Figures 5 and 6 for references to fields. Only basaltic compositions are plotted on the diagram, and gabbros are excluded. (B) Cr-Yb diagram for melt and residue compositions (Pearce and Parkinson, 1993) (see Fig. 5 for key to symbols). Field for Hole 786 boninites is from Murton et al. (1992). Only basaltic-composition Ingalls ophiolite samples are plotted, and gabbros are excluded. FMM—fertile MORB mantle.

(Fig. 9). Two samples, CR-327-2 from the Cle Elum Ridge fault zone and CA-38 from the roof pendent (Fig. 2), have Cr, Y, and Yb values that are similar to boninites from the Esmeralda Peaks unit and the Izu-Bonin forearc (Fig. 8); one also has a fertile MORB mantle–normalized pattern that is similar to the Esmeralda Peaks boninites and Izu-Bonin forearc boninites (Fig. 9).

Dikes Cutting Mylonitic Peridotite

Undeformed dikes of diabase and lesser gabbro cut the mylonitic lherzolite adjacent to the fault-bounded blocks of the Esmeralda Peaks unit (Fig. 4) (Miller, 1980, 1985). These dikes display variable hydrothermal alteration, and some are totally altered to rodingite (Pratt, 1958; Frost, 1973, 1975; Miller, 1980, 1985). The strikes of these dikes vary from approximately north-south to east-west (Fig. 4).

The dikes that cut the mylonitic lherzolite (Table 7) have the same trace-element systematics as the mafic Esmeralda Peaks samples (Figs. 5, 8 and 9). These samples are typically MORB, and two are transitional between MORB and IAT (Figs. 5 and 8). Two samples have high TiO_2 and FeO^T values that are similar to Fe-Ti basalts that are most commonly found at propagating spreading centers on mid-ocean ridges and back-arc basins (Table 7; Sinton et al., 1983; Pearce et al., 1994).

Ingalls Sedimentary Rocks

Smith (1904) first described the sedimentary rocks that stratigraphically overlie the volcanic and plutonic rocks of the Ingalls ophiolite complex. These rocks are mostly argillite, and they occur predominantly as fault-bounded blocks within the eastern portion of the Ingalls ophiolite complex (Fig. 3). Most of the argillite is massive, with minor interbeds of graywacke, pebble conglomerate, pebbly mudstone, chert, and ophiolitic breccia (Southwick, 1962, 1974; Miller, 1980, 1985; Mlinarevic et al., 2003; MacDonald et al., 2005). Southwick (1974) suggested that the Ingalls graywackes were derived from a mature island arc. The ophiolitic breccias consist mainly of mafic igneous or serpentinite clasts (Harper et al., 2003; MacDonald et al., 2005). Isolated boulders and some kilometer-scale outcrops of diabase or gabbro observed within the argillite have been interpreted as olistoliths (Harper et al., 2003).

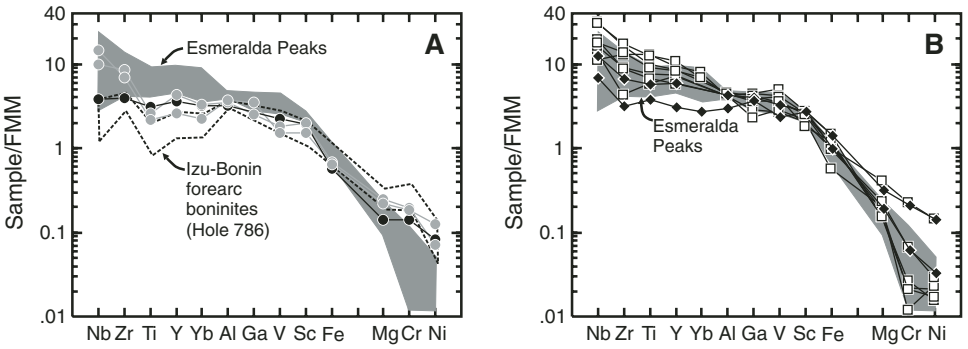

Figure 9. Fertile mid-ocean-ridge basalt (MORB) mantle–normalized diagrams (Pearce and Parkinson, 1993) for Ingalls ophiolite complex mafic samples. Esmeralda Peaks unit basalts and diabases are shown as the shaded field. Hole 786 boninites are from Murton et al. (1992). (A) Esmeralda Peaks boninites. (B) Dikes that cut mylonitic peridotite and dikes that cut amphibolites. See Figure 5 for key to symbols.

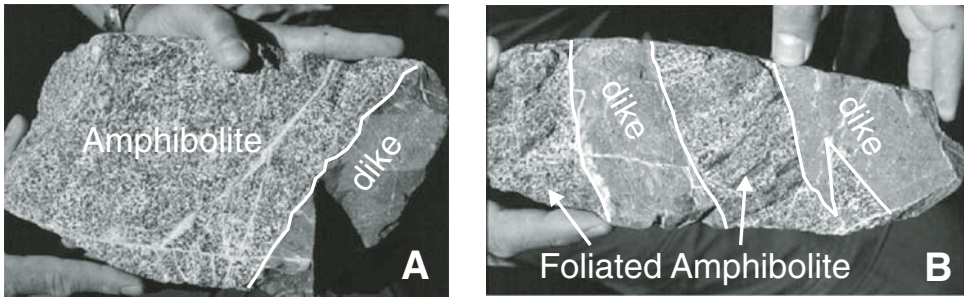

Figure 10. (A) Dike, on right side of the sample, that cuts an amphibolite that was originally a gabbro. (B) Two small dikes, right one showing a propagating tip, that cut a foliated amphibolite from the same locality as in A.

Depositional Age

Miller et al. (1993) reported Late Jurassic (probably Oxfordian or Kimmeridgian) radiolarian ages for cherts that overlie the Esmeralda Peaks unit (Table 3). Other Late Jurassic radiolarian assemblages, indicating an Upper Callovian to Lower-Middle Oxfordian age (superzone 1, zone 1H, through zone 2, subzone 2δ; Table 3; Pessagno et al., 1993), are reported from cherts that we collected from the Ingalls sedimentary rocks (E. Pessagno, 1999–2004, written commun.). These radiolarian cherts are interbedded with argillites and are probably low in the stratigraphic section. U-Pb ages of detrital zircons found within an Ingalls sandstone have a bimodal age distribution of 153 Ma and ca. 227 Ma; the 153 Ma peak age is interpreted as the approximate age of deposition (Miller et al., 2003).

The Late Jurassic age determinations are based on the radiolarian biostratigraphic time scale of Pessagno et al. (1993). Baumgartner et al. (1995) and Shervais et al. (2005a) have suggested that this time scale is incorrect. Using the time scale of Baumgartner et al. (1995), the Ingalls cherts range from early Bajocian to middle Oxfordian. However, the radiolarian ages based on Pessagno et al. (1993) fit the Late Jurassic time scale of Gradstein et al. (2004) and are consistent with the 161 ± 1 Ma zircon age for the mafic rocks beneath the cherts.

DISCUSSION

Tectonic Setting of the Iron Mountain Unit

The occurrences of basalt that has within-plate affinities (Figs. 6 and 7B), limestone, and abundant locally derived basaltic breccias are all consistent with a seamount origin for the Iron Mountain unit. The transitional within-plate basalt–E-MORB composition of the unit and its tholeiitic composition (Figs. 5, 6, and 7B) suggest that the Iron Mountain seamount formed close to an active spreading ridge (Shervais, 1982; Pearce, 1996a; Harpp and White, 2001).

The Iron Mountain rhyolite fractionated from a magma derived from the same mantle that produced the basalts. Similar rhyolites are known from a few within-plate ocean-island settings (e.g., Harris, 1983; Geist et al., 1995, 1998; Pearce, 1996b). An Early Jurassic age (ca. 192 Ma) is assigned to the Iron Mountain unit based on U-Pb zircon and radiolarian ages.

Tectonic Setting of the Esmeralda Peaks Unit

Back-Arc Basin Setting of the Esmeralda Peaks Unit

The geochemical affinities of modern back-arc basins include N-MORB, E-MORB, IAT, and CAB (Figs. 5, 6, and 8) (e.g., Hawkins and Melchior, 1985; Hawkins et al., 1990; Falloon et al., 1992; Pearce et al., 1994; Leat et al., 2000; Fretzdorff et al., 2002; Hawkins, 2003; Pearce, 2003). The Esmeralda Peaks samples have transitional IAT-MORB, IAT, and MORB geochemical affinities and consistently plot within the fields defined by modern back-arc basins (Figs. 5, 6, and 8). They originated from a mantle source that was slightly enriched when compared to N-MORB and that apparently underwent a high percentage of the melting that typically occurs in suprasubduction-zone settings (Figs. 6, 7C, and 8B) (Pearce, 1982). The transitional IAT-MORB composition of the Esmeralda Peaks unit leads us to infer that the unit formed in a Late Jurassic back-arc basin setting.

The felsic plutonic samples are IAT and CAB (Fig. 6), and their Ta/Yb ratios indicate that they originated from the same mantle source as the mafic rocks of the Esmeralda Peaks unit (Fig. 6). These features imply that the felsic plutonic rocks were fractionated from the same magmas that produced the diabases and pillow basalts.

The arc source for the Late Jurassic sediments that overlie the Esmeralda Peaks unit (Southwick, 1974; Mlinarevic et al., 2003) is consistent with a back-arc basin setting for the Ingalls ophiolite complex. In addition, the Late Jurassic Quartz Mountain stock, Hicks Butte complex, and Indian Creek complex are located south of the ophiolite complex (Fig. 1) (Miller, 1989; Miller et al., 1993). These plutonic rocks have been interpreted as part of an active arc located outboard of the Late Jurassic Ingalls back-arc basin (Miller et al., 1993), and they further support a back-arc origin for the Esmeralda Peaks unit.

TABLE 6. ANALYSES OF INGALLS OPHIOLITE COMPLEX AMPHIBOLITES AND DIKES THAT CUT THEM

Sample:	CR-327–1	HUCK-7	HUCK-8A	CR-327–2	HUCK-8B
Rock type:	amphibolite	amphibolite	amphibolite	diabase dike[§§]	diabase dike[##]
Latitude:[†]	N47 32.547	N47 27.900	N47 27.934	N47 32.547	N47 27.934
Longitude:	W121 03.139	W121 00.422	W121 00.341	W121 03.139	W121 00.341
Magma type:[‡]	IAT-MORB	MORB	MORB	MORB	MORB
SiO_2	49.19	52.34	51.96	48.14	52.45
Al_2O_3	14.64	19.57	15.96	11.30	16.25
TiO_2	0.98	0.77	1.29	0.67	1.00
FeO^{T}[§]	8.47	8.08	10.06	12.55	8.92
MnO	0.18	0.15	0.18	0.22	0.16
MgO	9.87	4.16	6.65	12.43	7.45
CaO	14.41	10.06	9.29	13.01	9.54
Na_2O	2.06	3.98	4.10	1.51	3.86
K_2O	0.16	0.76	0.36	0.14	0.28
P_2O_5	0.03	0.13	0.15	0.03	0.08
Total[#]	100.00	100.00	100.00	100.00	100.00
LOI	0.72	0.91	1.00	0.65	1.18
Ba[††]	72	316	81	22	70
Rb	4	15	6	1	6
Sr	167	362	188	59	161
Y	18	20	41	12	23
Zr	25	52	92	29	61
Nb	4.00	1.30	6.32	1.38	2.51
Th	N.D.[‡‡]	2.00	N.D.	0.11	1.00
Pb	1.00	N.D.	N.D.	0.99	N.D.
Ga	14	15	19	15	16
Zn	61	59	86	105	53
Cu	41	14	6	44	5
Ni	109	59	61	296	68
V	304	171	255	185	255
Cr	204	231	164	539	157
Hf	N.D.	N.D.	N.D.	0.70	N.D.
Cs	N.D.	N.D.	N.D.	0.15	N.D.
Sc	58.00	35.01	45.16	42.38	42.14
Ta	N.D.	N.D.	N.D.	0.10	N.D.
U	N.D.	N.D.	N.D.	0.02	N.D.
La	5.00	0.00	15.05	1.67	8.03
Ce	10.00	12.00	20.07	4.09	16.05
Pr	N.D.	N.D.	N.D.	0.60	N.D.
Nd	N.D.	N.D.	N.D.	3.22	N.D.
Sm	N.D.	N.D.	N.D.	1.26	N.D.
Eu	N.D.	N.D.	N.D.	0.72	N.D.
Gd	N.D.	N.D.	N.D.	1.73	N.D.
Tb	N.D.	N.D.	N.D.	0.33	N.D.
Dy	N.D.	N.D.	N.D.	2.14	N.D.
Ho	N.D.	N.D.	N.D.	0.46	N.D.
Er	N.D.	N.D.	N.D.	1.24	N.D.
Tm	N.D.	N.D.	N.D.	0.18	N.D.
Yb	N.D.	N.D.	N.D.	1.16	N.D.
Lu	N.D.	N.D.	N.D.	0.18	N.D.

[†]Lat/Long in hddd°mm.mmm' based on NAD27 CONUS datum.
[‡]Magma type determined using immobile trace-element discrimination diagrams. MORB—mid-ocean-ridge basalt, IAT-MORB—transitional island-arc tholeiite–mid-ocean-ridge basalt.
[§]FeO^{T}—total iron as FeO.
[#]Normalized to 100% loss on ignition (LOI) free.
[††]If all trace elements are reported, analysis of Y, Zr, Cr, V, and Ni was by X-ray fluorescence (XRF); others are by inductively coupled plasma–mass spectrometry (ICP-MS). Otherwise, all analysis was done by XRF.
[‡‡]N.D.—no data.
[§§]Diabase dike that cuts amphibolite CR-327–1.
[##]Diabase dike that cuts amphibolite HUCK-8A.

Esmeralda Peaks Boninites

Pearce and Parkinson (1993) used the fertile MORB mantle–normalized diagram in order to display mantle compositions and degrees of mantle melting that are independent of the subduction components that show up on chondrite- and N-MORB–normalized diagrams (Pearce, 1982; Plank and Langmuir, 1993). The fertile MORB mantle–normalized patterns for the three Esmeralda Peaks boninites suggest that they originated from a mantle source that underwent higher degrees of melting than other Esmeralda Peaks samples (Fig. 9A). High Cr and low Y and Yb values (Fig. 8) also suggest that the sources for these three samples underwent high degrees of mantle melting. The Esmeralda Peaks boninites have fertile MORB mantle–normalized patterns that are similar to the Izu-Bonin forearc boninites (Fig. 9A) (Murton et al., 1992). They also plot within or around the field for the Izu-Bonin forearc boninites on Figures

TABLE 7. ANALYSES OF MAFIC AND PLUTONIC SAMPLES THAT CUT MYLONITIC PERIDOTITE

Sample:	EL-84–2	HM-5	MS-56	MS-61	MS-64	MS-65–1	IOE-54A	MS-63–2	MS-38–1
Rock type:	diabase dike cuts plagioclase peridotite	diabase dike cuts mylonitic peridotite	diabase dike cuts mylonitic peridotite	diabase dike cuts mylonitic peridotite	diabase dike cuts mylonitic peridotite	diabase dike cuts mylonitic peridotite	diabase dike cuts mylonitic peridotite	trondhjemite cuts mylonitic peridotite	gabbro dike cuts mylonitic peridotite
Latitude:[†]	N47 25.087	N47 26.566	N47 26.889	N47 26.481	N47 26.223	N47 26.195	N47 26.062	N47 26.304	N47 25.902
Longitude:	W120 47.224	W120 59.471	W120 55.196	W120 55.287	W120 55.371	W120 55.356	W120 57.900	W120 55.385	W120 53.616
Magma type:[‡]	IAT-MORB	IAT-MORB	MO RB	IAT-MORB	IAT-MORB	MORB	MORB	VAG	MORB
SiO_2	43.66	58.79	46.98	50.90	51.59	41.50	46.22	77.55	48.65
Al_2O_3	15.88	15.45	16.47	15.17	15.06	15.34	16.59	0.12	16.38
TiO_2	2.11	1.13	1.70	1.29	2.17	0.98	1.57	13.65	0.98
FeO^{T}[§]	10.39	4.92	9.41	10.50	12.47	8.65	8.39	0.37	8.14
MnO	0.19	0.13	0.17	0.18	0.21	0.17	0.19	N.D.	0.15
MgO	5.78	7.45	6.93	5.78	5.73	15.26	9.00	0.25	9.09
CaO	21.58	5.61	10.50	9.83	7.53	17.73	15.90	0.36	13.58
Na_2O	0.17	6.30	7.44	4.29	4.90	0.31	1.49	7.59	2.85
K_2O	0.02	0.09	0.18	1.95	0.17	0.01	0.46	0.08	0.11
P_2O_5	0.22	0.12	0.22	0.11	0.18	0.05	0.18	0.03	0.06
Total[#]	100.00	100.00	100.00	100.00	100.00	100.00	100.00	100.00	100.00
LOI	3.75	2.16	4.01	0.95	2.16	5.45	2.64	0.38	2.50
Ba[††]	11	19	41	133	441	19	44	35	39
Rb	0	2	1	42	2	0	8	3	1
Sr	146	68	98	384	391	25	160	46	320
Y	41	22	32	28	35	27	31	7	22
Zr	155	79	147	80	115	39	123	78	35
Nb	5.90	3.79	6.09	3.21	2.13	2.69	3.52	8.79	0.75
Th	N.D.[‡‡]	N.D.	1.00	N.D.	0.43	2.99	0.19	7.99	0.03
Pb	2.00	N.D.	N.D.	1.00	0.43	2.99	0.37	5.99	0.38
Ga	15	9	16	17	17	11	14	10	15
Zn	82	71	67	72	89	60	45	3	48
Cu	34	60	71	83	47	34	10	7	62
Ni	8	46	34	31	41	289	58	10	109
V	309	215	266	317	377	205	269	14	248
Cr	24	29	51	64	53	549	164	N.D.	394
Hf	N.D.	N.D.	N.D.	N.D.	2.92	N.D.	2.85	N.D.	1.02
Cs	N.D.	N.D.	N.D.	N.D.	0.08	N.D.	0.90	N.D.	0.09
Sc	27.00	32.91	38.95	39.11	41.72	30.86	38.10	1.00	44.1
Ta	N.D.	N.D.	N.D.	N.D.	0.17	N.D.	0.26	N.D.	0.06
U	N.D.	N.D.	N.D.	N.D.	0.12	N.D.	0.09	N.D.	0.01
La	14.00	0.00	23.97	4.01	4.78	2.99	5.71	18.98	1.06
Ce	20.00	20.94	23.97	22.06	12.87	6.97	14.99	17.98	3.44
Pr	N.D.	N.D.	N.D.	N.D.	2.11	N.D.	2.23	N.D.	0.66
Nd	N.D.	N.D.	N.D.	N.D.	11.76	N.D.	11.53	N.D.	4.21
Sm	N.D.	N.D.	N.D.	N.D.	4.31	N.D.	3.83	N.D.	1.95
Eu	N.D.	N.D.	N.D.	N.D.	1.60	N.D.	1.50	N.D.	0.81
Gd	N.D.	N.D.	N.D.	N.D.	5.50	N.D.	4.86	N.D.	2.86
Tb	N.D.	N.D.	N.D.	N.D.	1.02	N.D.	0.88	N.D.	0.59
Dy	N.D.	N.D.	N.D.	N.D.	6.42	N.D.	5.70	N.D.	3.99
Ho	N.D.	N.D.	N.D.	N.D.	1.35	N.D.	1.18	N.D.	0.85
Er	N.D.	N.D.	N.D.	N.D.	3.69	N.D.	3.25	N.D.	2.39
Tm	N.D.	N.D.	N.D.	N.D.	0.53	N.D.	0.47	N.D.	0.34
Yb	N.D.	N.D.	N.D.	N.D.	3.25	N.D.	2.80	N.D.	2.09
Lu	N.D.	N.D.	N.D.	N.D.	0.50	N.D.	0.44	N.D.	0.32

[†]Lat/Long in hddd°mm.mmm' based on NAD27 CONUS datum.

[‡]Magma type determined using immobile trace-element discrimination diagrams. MORB—mid-ocean-ridge basalt, IAT-MORB—transitional island-arc tholeiite–mid-ocean-ridge basalt, VAG—volcanic-arc granite.

[§]FeO^{T}—total iron as FeO.

[#]Normalized to 100% loss on ignition (LOI) free.

[††]If all trace elements are reported, analysis of Y, Zr, Cr, V, and Ni was by X-ray fluorescence (XRF); others are by inductively coupled plasma–mass spectrometry (ICP-MS). Otherwise, all analysis was done by XRF.

[‡‡]N.D.—no data.

6 and 8. Crawford et al. (1989) and Deschamps and Lallemand (2003) suggested that boninite enrichment in Si, large ion lithophile elements, Cr, Ni, and light rare earth elements is the result of the melting of a refractory mantle source in the presence of a dehydrating slab. The Esmeralda Peaks samples display all of these geochemical characteristics described for boninites by Crawford et al. (1989) and Deschamps and Lallemand (2003) (Figs. 5, 6, 7D, 8, and 9A; Table 4), and thus they are inferred to have originated from second-stage melting of the mantle that produced the other Esmeralda Peaks samples. Second-stage melting is considered to be a common origin for boninites (van der Laan et al., 1989; Pearce et al., 1992).

Boninites only occur in suprasubduction-zone settings (Bloomer and Hawkins, 1983; Hawkins, 2003; Deschamps and Lallemand, 2003). They usually occur in forearcs, but they can also occur in back-arc basins (Bloomer and Hawkins, 1983; Hawkins, 2003; Deschamps and Lallemand, 2003). The boninites within the Esmeralda Peaks mafic unit were initiated by forearc rifting and most likely persisted after an outboard arc and back-arc basin had formed.

Geochemical Correlation of Mafic Units

The basalt and diabase of the Esmeralda Peaks unit have similar geochemical affinities (Figs. 5. 6, 7, and 8). This suggests that these rocks originated from the same mantle source. This geochemical correlation agrees with field observations that suggest that dikes cut and feed into the pillow basalts (Miller, 1980, 1985; Gray, 1982).

We suggest that the amphibolites, the dikes that cut them (Fig. 10), and the dikes that cut the mylonitic lherzolite (Fig. 4) are related to the Esmeralda Peaks unit. The geochemical affinities of these rocks are very similar to those of the Esmeralda Peaks unit (Figs. 5, 8, and 9B). Fertile MORB mantle patterns suggest that all of the mafic rocks, including the boninites, originated from a similar mantle source (Fig. 9).

Fracture-Zone Setting for the Late Jurassic Esmeralda Peaks Unit

The fracture-zone interpretation of the Navaho Divide fault zone and the Ingalls ophiolite complex was based on a number of features in the complex that are analogous to those of modern fracture zones: (1) The juxtaposition of two petrologically distinct mantle peridotites by a fault zone (Fig. 3) (e.g., Hayes transform; Smith, 1994) (Miller, 1985; Miller and Mogk, 1987; Schultz et al., 2005); (2) the mineral chemistry, geothermometry, and microstructures of the high-temperature mylonitic ultramafites (Miller and Mogk, 1987); (3) locally derived ophiolitic breccia and sedimentary serpentinite (e.g., Romanche and Ecuador fracture zones; Bonatti et al., 1973; Anderson and Nishimori, 1979) (Miller, 1985; MacDonald et al., 2005); (4) dikes of diabase and gabbro that cut serpentinized peridotite (Fig. 4) (e.g., Kane fracture zone; Fox and Gallo, 1984; Tartarotti et al., 1995); and (5) amphibolites that are deformed gabbros (Figs. 3 and 10) (e.g., Vema fracture zone; Honnorez et al., 1984) (Miller, 1985). The geochemical similarities between the amphibolites, the dikes that cut them, and the dikes that cut the mylonitic peridotite with the Esmeralda Peaks unit suggest that the fracture zone that disrupted the mafic units of the Ingalls ophiolite complex was active in the Late Jurassic.

An alternative interpretation for the Navaho Divide fault zone could be a fossil subduction zone. Boninites, like those of the Esmeralda Peaks unit, are commonly found within forearcs associated with oceanic subduction zones (Stern and Bloomer, 1992; Hawkins, 2003; Stern, 2002). Also, seamounts, the interpreted setting for the Iron Mountain unit (MacDonald et al., this volume, chapter 5), are found in fossil subduction zones (e.g., Snow Mountain complex; MacPherson, 1983). However, the Navaho Divide fault zone, as well as the rest of the Ingalls complex, lacks the high-pressure, low-temperature metamorphism found within fossil subduction zones (Ernst, 1973). This fact, along with the findings outlined previously, leads us to favor a fracture-zone over a subduction-zone setting for the Navaho Divide fault zone.

Polygenetic Origin of the Ingalls Ophiolite Complex

Miller et al. (1993), Metzger et al. (2002), and Harper et al. (2003) all suggested a back-arc basin origin for the Ingalls ophiolite complex. We agree with these researchers; however, the new geochemical and age data for the Ingalls ophiolite complex allow us to further constrain this tectonic setting.

The Ingalls ophiolite complex is polygenetic. The Early Jurassic component, the Iron Mountain unit, originated as a shallow-water, intraplate off-axis seamount (MacDonald et al., 2002, this volume, chapter 5). These Early Jurassic rocks were subsequently rifted apart during the Late Jurassic to form the ophiolitic basement of the rift-facies, Late Jurassic Esmeralda Peaks unit (Fig. 11). The Late Jurassic rocks originated in a back-arc basin setting and were deformed by a fracture zone (Miller and Mogk, 1987; MacDonald et al., 2005). Faulting in this back-arc–fracture zone formed the large-scale serpentinite mélange within which lie the crustal units of the ophiolite (Miller, 1985).

Regional Correlation of the Ingalls Ophiolite Complex

Comparison of Sedimentary Rocks

Sandstones from the Late Jurassic Galice Formation, which overlies the Josephine ophiolite (Fig. 11), have similar compositions to sandstones from the Late Jurassic Ingalls sedimentary rocks (Table 8) (Southwick, 1962, 1974; MacDonald et al., 2006). Detrital zircons from one Galice Formation and one Ingalls sandstone have comparable bimodal age distributions (153 Ma and ca. 227 Ma; Fig. 11), and similar age-corrected $^{143}Nd/^{144}Nd$ values (0.51278 ± 1 and 0.51273 ± 1, respectively; Miller et al., 2003). The Late Jurassic cherts from the Galice Formation contain Radiolaria that are identical to those within Ingalls cherts (Fig. 11) (E. Pessagno, 1999–2004, written commun.).

The Middle Jurassic Coast Range ophiolite (Fig. 1) is overlain by tuffaceous chert and mudstone, which is in turn overlain

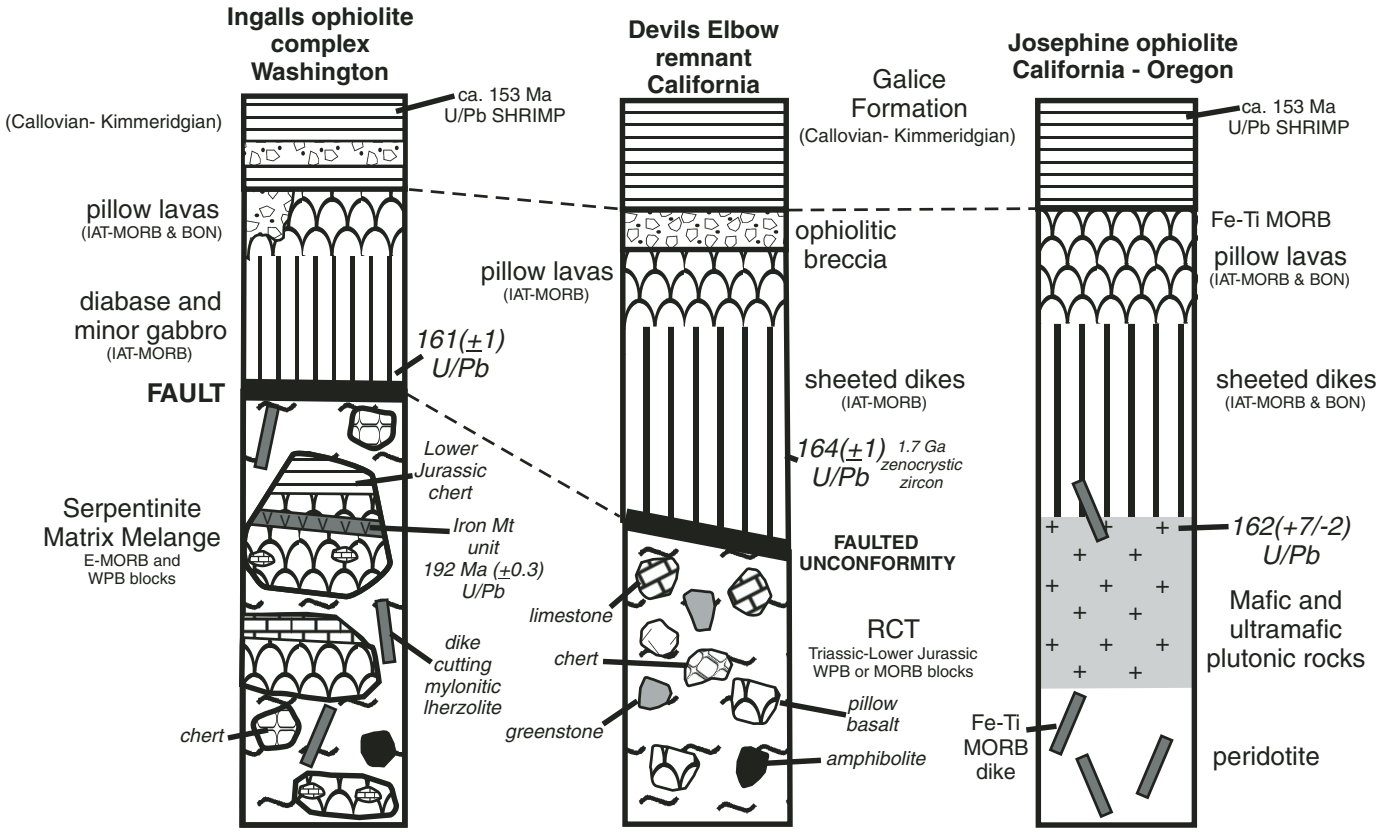

Figure 11. Tectonostratigraphy of the Ingalls ophiolite complex, Devils Elbow remnant of the Josephine ophiolite and underlying Rattlesnake Creek terrane (RCT), and the Josephine ophiolite. See text for discussion of fossil and U-Pb zircon ages and chemical affinities. Devils Elbow remnant and Josephine ophiolite were modified from Harper et al. (1994) and Wright and Wyld (1994). IAT—island-arc tholeiite; WPB—within-plate basalt; MORB—mid-ocean-ridge basalt; BON—boninite; E—enriched; N—normal; SHRIMP—sensitive high-resolution ion microprobe.

by the Great Valley Group (e.g., Hopson et al., 1981; Ingersoll, 1983; Robertson, 1990; Shervais et al., 2005a). Originally, an Oxfordian through Tithonian age was assigned to the tuffaceous chert and mudstone, and a Tithonian age was assigned to the overlying basal Great Valley Group (Imlay and Jones, 1970; Pessagno, 1977; Pessagno et al., 2000). This represents an ~9 m.y. depositional hiatus between the Coast Range ophiolite and the sedimentary rocks that overlie it (Hopson et al., 1996; Pessagno et al., 2000). The oldest radiolarian assemblages in the sediments above the Coast Range ophiolite originated from an equatorial paleo-environment (Hopson et al., 1996; Pessagno et al., 2000). This differs from the more northern paleo-environment inferred for the oldest radiolarian assemblages within the Galice Formation (Pessagno et al., 1993, 2000; Pessagno, 2006), and the comparable Ingalls sedimentary rocks (Table 8).

Shervais et al. (2005a), using Baumgartner et al.'s (1995) Unitary Association radiolarian zones, reinterpreted the age of the tuffaceous chert and mudstone that depositionally overlie the Coast Range ophiolite. Shervais et al. (2005a) assigned a Bajocian age to the oldest radiolarians and suggested that no depositional hiatus exists between the tuffaceous chert and mudstone and underlying Coast Range ophiolite. They also correlated these rocks with the Galice Formation by reassigning a Bajocian age to the lowest members of the Galice Formation (Table 8) (see Shervais et al., 2005a, for discussion). This suggests that the tuffaceous chert and mudstone that overlie the Coast Range ophiolite may also correlate with the Ingalls sedimentary rocks *if* the radiolarian zones of Baumgartner et al. (1995) are correct *and if* the radiolarian zones of Pessagno et al. (1993) are incorrect (Table 8). It should be noted that Gradstein et al. (2004) suggest that there are large uncertainties for the Late Jurassic time scale.

The sedimentary rocks that occur within and unconformably overlie the Fidalgo Igneous Complex, a Middle Jurassic ophiolite and intruding island-arc complex located within the San Juan Islands, Washington (Fig. 1) (Brown et al., 1979; Brandon et al., 1988), are the informal Trump unit and Lummi Group, respectively (Garver, 1988a). These sediments are Tithonian or younger in age, and sandstones from the Trump unit and Lummi Group have different compositions than Ingalls sandstones (Table 8) (Southwick,

TABLE 8. COMPARISON OF THE INGALLS OPHIOLITE COMPLEX WITH THE JOSEPHINE, COAST RANGE, AND FIDALGO OPHIOLITES

Ophiolite	Age	Polygenetic	Geochemical affinities of basaltic rocks	Overlying sedimentary rocks correlate with:
Ingalls[†]	160–162 Ma, 192 Ma[††]	Yes	IAT-MORB [‡‡], IAT, MORB, WPB[††], BON	Rocks on Josephine; may correlate with rocks on Coast Range
Josephine and its rift facies[‡]	160–169 Ma	Yes	IAT-MORB [‡‡], IAT, MORB, BON	Rocks on Ingalls; may correlate with rocks on Coast Range
Coast Range[§]	164–170 Ma (and younger ages)	No	IAT-MORB[‡‡], IAT, MORB, WPB, BON	Rocks on Fidalgo; may correlate with rocks on Ingalls and Josephine
Fidalgo[#]	≥155–162 Ma	No	MORB[‡‡] (6 samples)	Rocks on Coast Range.

Note: MORB—mid-ocean-ridge basalt, IAT-MORB—transitional island-arc tholeiite–mid-ocean-ridge basalt, WPB—within-plate basalt; BON—boninite.

[†]Miller et al. (1993), Metzger et al. (2002), Miller et al. (2003), MacDonald et al. (Chapter 5).

[‡]Harper (1984), Pinto-Auso and Harper (1985), Wright and Wyld (1986), Saleeby (1990), Harper et al. (1994), Palfy et al. (2000), Harper (2003a, 2003b), Miller et al. (2003), Yule et al. (2006).

[§]Menzies et al. (1977), Hopson et al. (1981), Shervais and Kimbrough (1985), Lagabrielle et al. (1986), Shervais (1990), Giaramita et al. (1998), Kosanke (2000), Shervais et al. (2004), Shervais et al. (2005a, 2005b).

[#]Whetten et al. (1978, 1980), Garver (1988a, 1988b), Brandon et al. (1988).

[††]Age of the Iron Mountain unit, the rifted basement of the Ingalls.

[‡‡]Major geochemical affinity.

1962, 1974; Garver, 1988a). The Lummi Group has been correlated to the Great Valley Group by Garver (1988b) (Table 8).

The sedimentary rocks associated with the Ingalls ophiolite complex, Coast Range ophiolite, and Fidalgo Igneous Complex do not display the Late Jurassic deformation attributed to the Nevadan orogeny. In contrast, the Galice Formation displays Nevadan deformation (Harper, 1984, 2006; Wyld and Wright, 1988; Harper et al., 1994). Numerous syn-Nevadan dikes intrude the Galice Formation but are absent in the sediments associated with the Ingalls, Coast Range, and Fidalgo ophiolites (Harper et al., 1994; Harper, 2006). Sandstone of the Galice Formation has Precambrian detrital zircons (Miller and Saleeby, 1995; Miller et al., 2003), while the Ingalls sandstone does not (Miller et al., 2003). The Ingalls sedimentary rocks also lack the metalliferous sediments that are located near the contact between the Galice Formation and Josephine ophiolite (Pinto-Auso and Harper, 1985).

Time Relations of Ophiolites

The age of the Esmeralda Peaks unit is 161 ± 1 Ma (Table 8) (U-Pb zircon; Miller et al., 2003). The U-Pb zircon age of the older rifted basement to the Esmeralda Peaks unit, the Iron Mountain unit, is 192 ± 0.3 Ma (Table 8). Radiolaria in cherts interbedded with pillow basalts of the Iron Mountain unit have Early Jurassic ages (Table 3). Similar Jurassic ages occur in other ophiolites within the North American Cordillera (Fig. 1).

Harper et al. (1994) reported a U-Pb zircon age of 162 ± 1 Ma from the Josephine ophiolite (Fig. 1); however, Palfy et al. (2000) recalculated this age to 162 +7/–2 Ma based on the lack of duplicate concordant fractions and apparent Pb loss (Table 8). The rift facies of the Josephine ophiolite, the Devils Elbow and Preston Peak ophiolites (Fig. 1), both have U-Pb zircon ages of ca. 164 Ma (Fig. 11) (Wright and Wyld, 1986; Saleeby, 1990).

The rifted basement of the Josephine ophiolite rift facies, the Rattlesnake Creek terrane (Fig. 1), consists of a serpentinite-matrix mélange basement and volcanic cover sequence (Wright and Wyld, 1994; Yule et al., 2006). Fossils from the mélange have Paleozoic, Late Triassic, and Early Jurassic ages (Fig. 11) (Edelman et al., 1989; Saleeby, 1990; Wright and Wyld, 1994, and references within). Fossils from the volcanic cover sequence yield Late Triassic and Early Jurassic ages (Edelman et al., 1989; Saleeby, 1990; Wright and Wyld, 1994, and references within). The mélange and cover sequence of the Rattlesnake Creek terrane are intruded by 193–207 Ma plutons (U-Pb zircon) (Wright and Wyld, 1994).

The Fidalgo Igneous Complex (Fig. 1) has yielded generally discordant U-Pb zircon ages ranging from 170 to 160 Ma (Whetten et al., 1978, 1980). These dates are from the island-arc complex and represent the minimum age of the ophiolitic rocks of the Fidalgo Igneous Complex (Brandon et al., 1988). Radiolaria from chert interbedded with pillow basalts of the ophiolitic rocks are Middle to Late Jurassic in age (Table 8) (Garver, 1988a; Brandon et al., 1988, and references within).

U-Pb zircon ages for the Coast Range ophiolite (Fig. 1) mostly range between 164 and 173 Ma (Table 8) (Hopson et al., 1981; Mattinson and Hopson, 1992; Shervais et al., 2005a), although ages as young as 144–148 Ma, 152–153 Ma, and ca. 156 Ma have been reported from different remnants of the ophiolite (Hopson et al., 1981). U-Pb zircon ages from two remnants of the Coast Range ophiolite in Oregon (Fig. 1) are ca. 169 Ma (Saleeby, 1984) and 163–164 Ma (Saleeby, 1999, written commun. to Kosanke [2000]; Harper et al., 2002).

Comparison of Geochemical Affinities

The Josephine ophiolite and Coast Range ophiolite have transitional IAT-MORB geochemical affinities, similar to those of the Esmeralda Peaks unit (Fig. 12; Table 8) (Menzies et al., 1977; Harper, 1984, 2003a, 2003b; Lagabrielle et al., 1986; Shervais, 1990; Coulton et al., 1995; Giaramita et al., 1998; Kosanke, 2000; Metzger et al., 2002). The Josephine ophiolite, Coast Range ophiolite, and Esmeralda Peaks unit all contain boninites or "boninitic" affinity lavas (Table 8) (Shervais and Kimbrough, 1985; Lagabrielle et al., 1986; Shervais, 1990; Giaramita et al., 1998; Kosanke, 2000; Metzger et al., 2002; Harper, 2003a). Dikes that cut the mylonitic peridotite in the

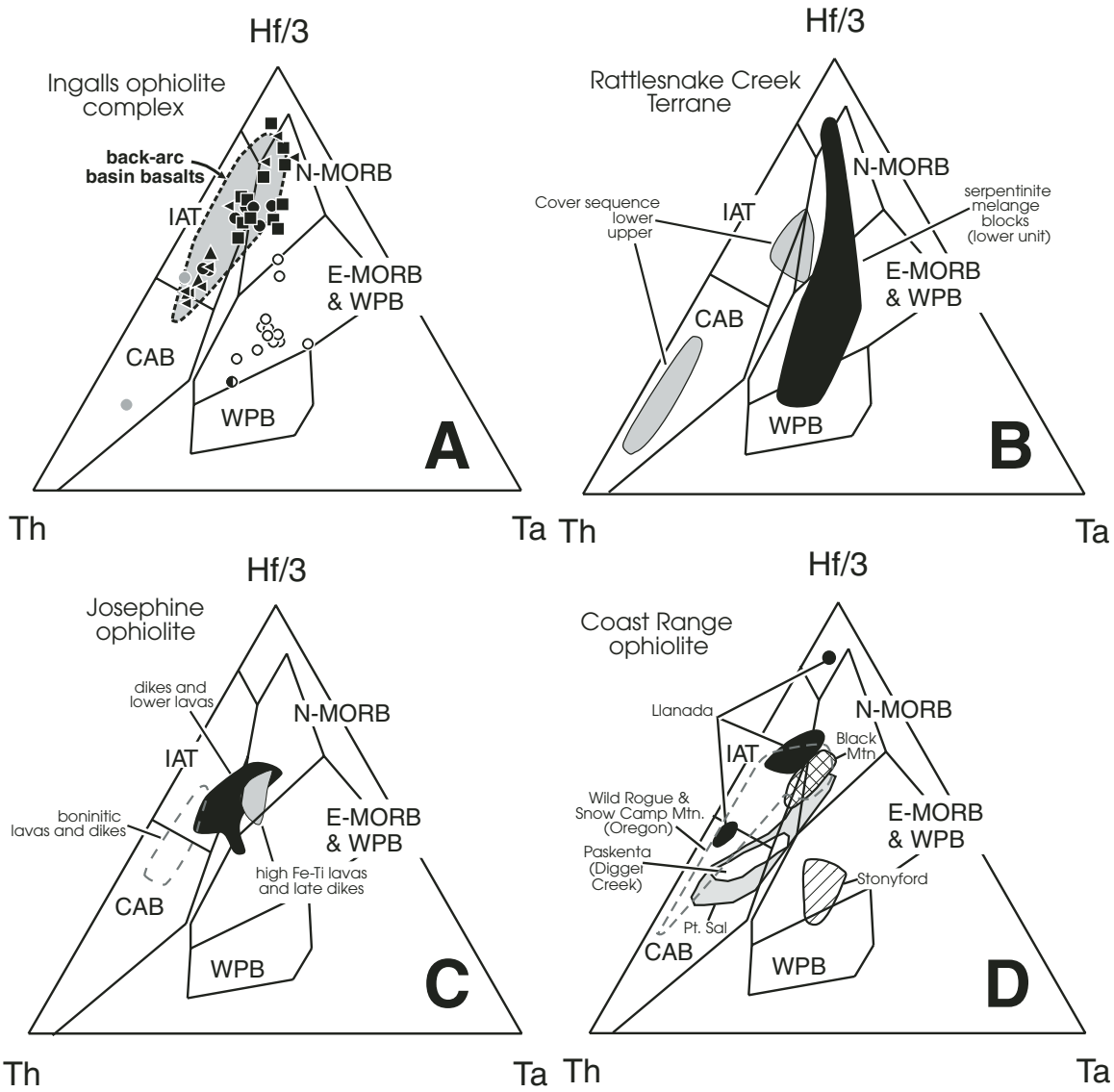

Figure 12. Ta-Hf-Th discrimination diagram of Wood (1980). (A) Ingalls ophiolite samples and field (see Fig. 5 for key to symbols) for back-arc basins (see Fig. 5 for compilation). Esmeralda Peaks gabbros (sideways triangles) are plotted because fractionation and crystal accumulation does not significantly change the ratios of these elements. (B) Rattlesnake Creek terrane (Wright and Wyld, 1994). (C) Josephine ophiolite (references given in text). (D) Coast Range ophiolite (references given in text). IAT—island-arc tholeiite; WPB—within-plate basalt; MORB—mid-ocean-ridge basalt; BON—boninite; E—enriched; N—normal; CAB—calc-alkaline basalt.

Esmeralda Peaks unit (Fig. 4) have Fe and Ti values that trend to Fe-Ti basalt compositions (Fig. 5; Table 7). Fe-Ti basalts are found in the late dikes and lava flows of the Josephine ophiolite (Harper, 2003b) and the fourth-stage volcanic rocks of the Coast Range ophiolite (Shervais, 2001; Shervais et al., 2004).

The late stage of the Stonyford volcanic complex of the Coast Range ophiolite and blocks of basalt in the Rattlesnake Creek mélange have within-plate basalt affinities that are transitional to E-MORB and tholeiitic-alkaline compositions (Fig. 12; Table 8) (Wright and Wyld, 1994; Shervais et al., 2005b; Yule et al., 2006). These within-plate basalt compositions are similar to those of the Iron Mountain unit (Fig. 12; Table 8); however, the within-plate basalt–affinity rocks of the Stonyford complex are ~28 m.y. younger than those of the Iron Mountain unit (Fig. 12), whereas the within-plate basalt–affinity rocks of the Rattlesnake Creek terrane are similar in age (Figs. 11 and 12).

CONCLUSIONS

Our main conclusions are that: (1) the Galice Formation and Ingalls sedimentary rocks are correlative (Fig. 11; Table 8); (2) the Late Jurassic Esmeralda Peaks unit of the Ingalls complex

is a rift-edge facies of the Josephine ophiolite (Fig. 11); (3) the rift-edge facies of the Josephine ophiolite—the Devils Elbow ophiolite (Wyld and Wright, 1988), the rift-edge facies along the northern margin of the Josephine ophiolite (Yule et al., 2006), and the Preston Peak ophiolite (Fig. 11) (Snoke, 1977; Saleeby et al., 1982)—correlate with the Esmeralda Peaks unit; and (4) the Iron Mountain unit is the rifted basement of the Esmeralda Peaks unit, and it is broadly correlative with the rifted basement of the Josephine ophiolite, the Rattlesnake Creek terrane (Fig. 11).

The initial rifting that formed the Late Jurassic Ingalls back-arc basin likely originated in the forearc, based on the presence of boninites within the Esmeralda Peaks unit, although boninitic rocks also rarely occur in back-arc basin settings (Pearce et al., 1994; Hawkins, 2003; Deschamps and Lallemand, 2003). Harper (2003a) suggested that initial rifting of the Josephine back-arc basin, which we correlate to the Ingalls back-arc basin, occurred in the forearc. A transform fault/fracture zone was located within the Ingalls back-arc basin (Miller and Mogk, 1987; MacDonald et al., 2005).

The Late Jurassic plutons, located south of the Ingalls ophiolite complex (Fig. 1), have been interpreted as a potential outboard active arc to the Late Jurassic Ingalls basin (Miller et al., 1993; Harper et al., 2003; MacDonald, 2006). This arc complex has also been correlated to the Rogue-Chetco arc complex (Miller et al., 1993; MacDonald, 2006), which has been interpreted to be the outboard active arc for the Late Jurassic Josephine basin (Saleeby et al., 1982; Harper et al., 1994).

Based on these correlations, and Wyld et al.'s (2006) reconstruction that places the Ingalls ophiolite complex close to the Josephine ophiolite in the Late Cretaceous, we suggest that these two ophiolites occupied different parts of the same oceanic back-arc basin, adjacent to the western coast of North America in the Jurassic. The Ingalls ophiolite complex, however, lacks Nevadan deformation and was not intruded by Late Jurassic calc-alkaline igneous rocks, in contrast to the Josephine ophiolite, thus suggesting that there was some distance between these ophiolites during their formation. Subsequently, the Ingalls ophiolite complex may have been displaced farther from the Josephine ophiolite, and its outliers, by dextral strike-slip faulting. This interpretation requires much smaller displacement for the Ingalls ophiolite complex, and the Mount Stuart batholith that intrudes it (Figs. 2 and 3), than the paleomagnetic data suggest (300–800 km versus ≈3000 km, respectively; Beck et al., 1981; Ague and Brandon, 1996; Butler et al., 2001; Housen et al., 2003; Wyld et al., 2006). Alternatively, the Josephine basin could have continued northward for ~440 km.

ACKNOWLEDGMENTS

This paper is dedicated to Cliff Hopson for his recognition of the significance of Jurassic ophiolitic and arc rocks in the Washington Cascades, and we thank him for his enthusiasm and encouragement of our research over the past 30 yr. This research was supported by National Science Foundation (NSF) grant EAR-0003444 to G.D. Harper and NSF grant EAR-0087829 to R.B. Miller and J.S. Miller, State University of New York (SUNY) Albany FRAP grant to G.D. Harper, and U.S. Geological Survey EDMAP award 03HQAG0066 to R.B. Miller. J.H. MacDonald was funded by Geological Society of America (GSA) Research Grant 6951-01, a Sigma Xi Grant-in-Aid of Research, and the Department of Earth and Atmospheric Science, SUNY Albany. E. Pessagno did outstanding work in identifying radiolarians. Robert Stern, Yildrem Dilek, and John Shervais provided us with critical reviews that greatly improved the quality of this paper. John Shervais and Jim Wright proved to be first class editors of this volume. Bill Kidd reviewed an early draft of this paper. J. Arnason, B. Fletcher, and K. Hollocher assisted greatly with inductively coupled plasma–mass spectrometry (ICP-MS) analysis at Union College. We thank Scott McPeek, Mike Siudy, Ron Karpowicz, and James Donohue for assistance in the field, Dan Redell for assistance with sample preparation, and the 2003 GSA National Meeting Ingalls Ophiolite field trip participants for their stimulating discussions.

REFERENCES CITED

Ague, J.J., and Brandon, M.T., 1996, Regional tilt of the Mount Stuart batholith, Washington, determined using aluminum-in-hornblende barometry: Implications for northward translation of Baja British Columbia: Geological Society of America Bulletin, v. 108, p. 471–488, doi: 10.1130/0016-7606(1996)108<0471:RTOTMS>2.3.CO;2.

Anderson, R.N., and Nishimori, R.K., 1979, Gabbro, serpentinite, and mafic breccia from the East Pacific: Journal of Physics of the Earth, v. 27, p. 467–480.

Baumgartner, P.O., Bartolini, A., Carter, E.S., Conti, M., Cortese, G., Danelian, T., De Wever, P., Dumitrica, P., Dumitrica-Jud, R., Gorican, S., Guex, J., Hull, D.M., Kito, N., Marcucci, M., Matsuoka, A., Murchey, B.L., O'Dogherty, L., Savary, J., Vishnevskaya, V., Widz, D., and Yao, A., 1995a, Middle Jurassic to Early Cretaceous radiolarian biochoronology of Tethys based on Unitary Associations, *in* Baumgartner, P.O., O'Dogherty, L., Gorican, S., Urquhart, E., Pillevuit, A., and De Wever, P., eds., Middle Jurassic to Lower Cretaceous Radiolaria of Tethys: Occurrences, Systematics, Biochronology: Lausanne, Switzerland, Memoires de Geologie (Lausanne): p. 1013–1048.

Beccaluva, L., and Serri, G., 1988, Boninitic and low-Ti subduction-related lavas from intraoceanic arc-backarc systems and low-Ti ophiolites; a reappraisal of their petrogenesis and original tectonic setting: Tectonophysics, v. 146, p. 291–315, doi: 10.1016/0040-1951(88)90097-2.

Beck, M.E., Jr., Burmester, R.F., and Schoonover, R., 1981, Paleomagnetism and tectonics of the Cretaceous Mt. Stuart batholith of Washington: Translation or tilt?: Earth and Planetary Science Letters, v. 56, p. 336–342, doi: 10.1016/0012-821X(81)90138-2.

Berndt, M.E., Seyfried, W.E., Jr., and Beck, J.W., 1988, Hydrothermal alteration processes at mid-ocean ridges; experimental and theoretical constraints from Ca and Sr exchange reactions and Sr isotopes ratios: Journal of Geophysical Research, v. 93, p. 4573–4583.

Bloomer, S.H., 1983, Distribution and origin of igneous rocks from the landward slopes of the Mariana Trench; implications for its structure and evolution: Journal of Geophysical Research, v. 88, p. 7411–7428.

Bloomer, S.H., and Hawkins, J.W., 1983, Gabbroic and ultramafic rocks from the Mariana Trench; an island arc ophiolite, *in* Hayes, D.E., ed., The Tectonic and Geologic Evolution of Southeast Asian Seas and Islands: Part 2: American Geophysical Union Geophysical Monograph 27, p. 294–317.

Bonatti, E., Honnorez, J., and Gartner, S., Jr., 1973, Sedimentary serpentinites from the Mid-Atlantic Ridge: Journal of Sedimentary Petrology, v. 43, p. 728–735.

Brandon, M.T., Cowan, D.S., and Vance, J.A., 1988, The Late Cretaceous San Juan Thrust System, San Juan Islands, Washington: Geological Society of America Special Paper 221, 81 p.

Brown, E.H., 1987, Structural geology and accretionary history of the Northwest Cascades system, Washington and British Columbia: Geological Society of America Bulletin, v. 99, p. 201–214, doi: 10.1130/0016-7606(1987)99<201:SGAAHO>2.0.CO;2.

Brown, E.H., Bradshaw, J.Y., and Mustoe, G.E., 1979, Plagiogranite and keratophyre in ophiolite on Fidalgo Island, Washington: Geological Society of America Bulletin, v. 90, p. 493–507, doi: 10.1130/0016-7606(1979)90<493:PAKIOO>2.0.CO;2.

Butler, R.F., Gehrels, G.E., and Kodama, K.P., 2001, A moderate translation alternative to the Baja British Columbia hypothesis: GSA Today, v. 11, no. 6, p. 4–10, doi: 10.1130/1052-5173(2001)011<0004:AMTATT>2.0.CO;2.

Cameron, W.E., Nisbet, E.G., and Dietrich, V.J., 1980, Petrographic dissimilarities between ophiolitic and ocean-floor basalts, *in* Panayiotiou, A., ed., Ophiolites: Proceedings International Ophiolite Conference: Nicosia, Geological Survey of Cyprus, p. 182–192.

Cann, J.R., 1970, Rb, Sr, Y, Zr and Nb in some ocean floor basaltic rocks: Earth and Planetary Science Letters, v. 10, p. 7–11, doi: 10.1016/0012-821X(70)90058-0.

Coulton, A.J., Harper, G.D., and O'Hanley, D.S., 1995, Oceanic versus emplacement-age serpentinization in the Josephine ophiolite: Implications for the nature of the Moho at intermediate and slow spreading ridges: Journal of Geophysical Research, v. 100, p. 22,245–22,260, doi: 10.1029/95JB02157.

Crawford, A.J., Falloon, T.J., and Green, D.H., 1989, Classification, petrogenesis and tectonic setting of boninites, *in* Crawford, A.J., ed., Boninites: London, Unwin Hyman, p. 1–49.

Deschamps, A., and Lallemand, S., 2003, Geodynamic setting of Izu-Bonin-Mariana boninites, *in* Larter, R.D., and Leat, P.T., eds., Intra-Oceanic Subduction Systems: Tectonic and Magmatic Processes: Geological Society [London] Special Publication 219, p. 163–185.

Dewey, J.F., and Bird, J.M., 1971, Origin and emplacement of the ophiolite suite: Appalachian ophiolites in Newfoundland: Journal of Geophysical Research, v. 76, p. 3179–3206.

Dickinson, W.R., Hopson, C.A., Saleeby, J.B., Schweickert, R.A., Ingersoll, R.V., Pessagno, E.A., Jr., Mattinson, J.M., Luyendyk, B.P., Beebe, W., Hull, D.M., Munoz, I.M., and Blome, C.D., 1996, Alternate origins of the Coast Range ophiolite (California): Introduction and implications: GSA Today, v. 6, no. 2, p. 1–10.

Dilek, Y., 1989a, Tectonic significance of post-accretion rifting of a Mesozoic island-arc terrane in the northern Sierra Nevada, California: The Journal of Geology, v. 97, p. 503–518.

Dilek, Y., 1989b, Structure and tectonics of an early Mesozoic oceanic basement in the northern Sierra Nevada metamorphic belt, California; evidence for transform faulting and ensimatic arc evolution: Tectonics, v. 8, p. 999–1014.

Edelman, S.H., Day, H.W., Moores, E.M., Zigan, S.M., Murphy, T.P., and Hacker, B.R., 1989, Structure across a Mesozoic Ocean-Continent Suture Zone in the Northern Sierra Nevada, California: Geological Society of America Special Paper 224, 56 p.

Ernst, W.G., 1973, Blueschist metamorphism and *P-T* regimes in active subduction zones: Experimental petrology and global tectonics: Tectonophysics, v. 17, p. 255–272, doi: 10.1016/0040-1951(73)90006-1.

Falloon, T.J., Malahoff, A., Zonenshain, L.P., and Bogdanov, Y., 1992, Petrology and geochemistry of back-arc basin basalts from Lau Basin spreading ridges at 15, 18 and 19S: Mineralogy and Petrology, v. 47, p. 1–35, doi: 10.1007/BF01165295.

Fox, P.J., and Gallo, D.G., 1984, A tectonic model for ridge-transform-ridge plate boundaries; implications for the structure of oceanic lithosphere: Tectonophysics, v. 104, p. 205–242, doi: 10.1016/0040-1951(84)90124-0.

Fretzdorff, S., Livermore, R.A., Devey, C.W., Leat, P.T., and Stoffers, P., 2002, Petrogenesis of the back-arc East Scotia Ridge, South Atlantic Ocean: Journal of Petrology, v. 43, p. 1435–1467, doi: 10.1093/petrology/43.8.1435.

Frost, B.R., 1973, Contact Metamorphism of the Ingalls Ultramafic Complex at Paddy-Go-Easy Pass, Central Cascades, Washington [Ph.D. thesis]: Seattle, Washington, University of Washington, 166 p.

Frost, B.R., 1975, Contact metamorphism of serpentinite, chlorite blackwall and rodingite at Paddy-Go Easy Pass, central Cascades, Washington: Journal of Petrology, v. 16, p. 272–313.

Garver, J.I., 1988a, Stratigraphy, depositional setting, and tectonic significance of the clastic cover to the Fidalgo ophiolite, San Juan Islands, Washington: Canadian Journal of Earth Sciences, v. 25, p. 417–432.

Garver, J.I., 1988b, Fragment of the Coast Range ophiolite and the Great Valley Sequence in the San Juan Islands, Washington: Geology, v. 16, p. 948–951, doi: 10.1130/0091-7613(1988)016<0948:FOTCRO>2.3.CO;2.

Geist, D., Howard, K.A., and Larson, P., 1995, The generation of oceanic rhyolites by crystal fractionation; the basalt-rhyolite association at Volcan Alcedo, Galapagos Archipelago: Journal of Petrology, v. 36, p. 965–982.

Geist, D., Naumann, T.R., and Larson, P., 1998, Evolution of Galapagos magmas; mantle and crustal fractionation without assimilation: Journal of Petrology, v. 39, p. 953–971, doi: 10.1093/petrology/39.5.953.

Giaramita, M., MacPherson, G.J., and Phipps, S.P., 1998, Petrologically diverse basalts from a fossil oceanic forearc in California; the Llanada and Black Mountain remnants of the Coast Range ophiolite: Geological Society of America Bulletin, v. 110, p. 553–571, doi: 10.1130/0016-7606(1998)110<0553:PDBFAF>2.3.CO;2.

Gradstein, F.M., Ogg, J.G., and Smith, A.G., eds., 2004, A Geologic Time Scale 2004: Cambridge, England, Cambridge University Press, 384 p.

Gray, J.E., 1982, Petrology and Geochemistry of the Eastern Portion of the Ingalls Complex, Central Washington Cascades [M.S. thesis]: Lawrence, Kansas, University of Kansas, 63 p.

Harper, G.D., 1984, The Josephine ophiolite, northwestern California: Geological Society of America Bulletin, v. 95, p. 1009–1026, doi: 10.1130/0016-7606(1984)95<1009:TJONC>2.0.CO;2.

Harper, G.D., 1995, Pumpellyosite and prehnitite associated with epidosite in the Josephine Ophiolite; Ca metasomatism during upwelling of hydrothermal fluids at a spreading axis, *in* Schiffman, P., and Day, H., eds., Low-Grade Metamorphism of Mafic Rocks: Geological Society of America Special Paper 296, p. 101–122.

Harper, G.D., 2003a, Tectonic implications of boninite, arc tholeiite, and MORB magma types in the Josephine ophiolite, California-Oregon, *in* Dilek, Y., and Robinson, P.T., eds., Ophiolites in Earth History: Geological Society [London] Special Publication 218, p. 207–229.

Harper, G.D., 2003b, Fe-Ti basalts and propagating-rift tectonics in the Josephine ophiolite: Geological Society of America Bulletin, v. 115, p. 771–787, doi: 10.1130/0016-7606(2003)115<0771:FBAPTI>2.0.CO;2.

Harper, G.D., 2006, Structure of syn-Nevadan dikes and their relationship to deformation of the Galice Formation, western Klamath terrane, northwestern California, *in* Snoke, A.W., and Barnes, C.G., eds., Geological Studies in the Klamath Mountains Province, California and Oregon: Geological Society of America Special Paper 410, p. 121–140.

Harper, G.D., and Wright, J.E., 1984, Middle to Late Jurassic tectonic evolution of the Klamath Mountains, California-Oregon: Tectonics, v. 3, p. 759–772.

Harper, G.D., Bowman, J.R., and Kuhns, R., 1988, Field, chemical, and isotopic aspects of submarine hydrothermal metamorphism of the Josephine ophiolite, Klamath Mountains, California-Oregon: Journal of Geophysical Research, v. 93, p. 4625–4657.

Harper, G.D., Saleeby, J.B., and Heizler, M., 1994, Formation and emplacement of the Josephine ophiolite and the Nevadan orogeny in the Klamath Mountains, California-Oregon; U-Pb zircon and $^{40}Ar/^{39}Ar$ geochronology: Journal of Geophysical Research, v. 99, no. B3, p. 4293–4321, doi: 10.1029/93JB02061.

Harper, G.D., Giaramita, M., and Kosanke, S., 2002, Field guide to the Josephine and Coast Range ophiolites, Oregon and California, *in* Moore, G.W., ed., Field Guide to Geologic Processes in Cascadia: Oregon Department of Geology and Mineral Industries Special Paper 36, p. 1–22.

Harper, G.D., Miller, R.B., MacDonald, J.H., Jr., Miller, J.S., and Mlinarevic, A.N., 2003, Evolution of a polygenetic ophiolite: The Jurassic Ingalls ophiolite, Washington Cascades, *in* Swanson, T.W., ed., Western Cordillera and Adjacent Areas: Boulder, Colorado, Geological Society of America, Field Guide 4, p. 251–265.

Harpp, K.S., and White, W.M., 2001, Tracing a mantle plume: Isotopic and trace element variations of Galapagos seamounts: Geochemistry, Geophysics, Geosystems, v. 2, doi: 10.1029/2000GC000137.

Harris, C., 1983, The petrology of lavas and associated plutonic inclusions of Ascension Island: Journal of Petrology, v. 24, p. 424–470.

Hawkins, J.W., 1995, Evolution of the Lau Basin: Insights from ODP Leg 135, *in* Taylor, B., and Natland, J., eds., Active Margins and Marginal Basins of the Western Pacific: American Geophysical Union Geophysical Monograph 88, p. 125–173.

Hawkins, J.W., 2003, Geology of supra-subduction zones—Implications for the origin of ophiolites, *in* Dilek, Y., and Newcomb, S., eds., Ophiolite Concept and the Evolution of Geological Thought: Geological Society of America Special Paper 373, p. 227–268.

Hawkins, J.W., and Melchior, J.T., 1985, Petrology of Mariana Trough and Lau Basin basalts: Journal of Geophysical Research, v. 90, p. 11,431–11,468.

Hawkins, J.W., Lonsdale, P.F., Macdougall, J.D., and Volpe, A.M., 1990, Petrology of the axial ridge of the Mariana Trough backarc spreading center: Earth and Planetary Science Letters, v. 100, p. 226–250, doi: 10.1016/0012-821X(90)90187-3.

Honnorez, J., Mevel, C., and Montigny, R., 1984, Occurrence and significance of gneissic amphibolites in the Vema fracture zone, equatorial Mid-Atlantic Ridge, *in* Gass, I.G., Lippard, S.J., and Shelton, A.W., eds., Ophiolites and Oceanic Lithosphere: Geological Society [London] Special Publication 13, p. 121–130.

Hopson, C.A., and Mattinson, J.M., 1973, Ordovician and Late Jurassic ophiolitic assemblages in the Pacific Northwest: Geological Society of America Abstracts with Programs, v. 5, no. 1, p. 57.

Hopson, C.A., Mattinson, J.M., and Pessagno, E.A., Jr., 1981, Coast Range ophiolite, western California, *in* Ernst, W.G., ed., The Geotectonic Development of California: Rubey Volume I: Englewood Cliffs, New Jersey, Prentice-Hall, p. 418–510.

Hopson, C.A., Pessagno, E.A., Jr., Mattinson, J.M., Luyendyk, B.P., Beebe, W., and Hull, D.M., Muñoz, I.M., and Blome, C.D., 1996, 2. Coast Range ophiolite as paleoequatorial mid-ocean lithosphere: GSA Today, v. 6, no. 2, p. 4–6.

Hopson, C.A., Mattinson, J., Pessagno, E., and Luyendyk, B., 2008, this volume, California Coast Range ophiolite: Composite Middle and Late Jurassic lithosphere, *in* Wright, J.E., and Shervais, J.W., eds., Ophiolites, Arcs, and Batholiths: A Tribute to Cliff Hopson: Geological Society of America Special Paper 438, doi: 10.1130/2008.2438(17).

Housen, B.A., Beck, M.E., Jr., Burmester, R.F., Fawcett, T., Petro, G., Sargent, R., Addis, K., Curtis, K., Ladd, J., Liner, N., Molitor, B., Montgomery, T., Mynatt, I., Palmer, B., Tucker, D., and White, I., 2003, Paleomagnetism of the Mount Stuart batholith revisited again: What has been learned since 1972?: American Journal of Science, v. 303, p. 263–299, doi: 10.2475/ajs.303.4.263.

Imlay, R.W., and Jones, D.L., 1970, Ammonites from the *Buchia* Zones in Northwestern California and Southwestern Oregon: U.S. Geological Survey Professional Paper P0647-B, 59 p.

Ingersoll, R.V., 1983, Petrofacies and provenance of late Mesozoic forearc basin, northern and central California: American Association of Petroleum Geologists Bulletin, v. 67, p. 1125–1142.

Kosanke, S.B., 2000, The Geology, Geochronology, Structure and Geochemistry of the Wild Rogue Wilderness Remnant of the Coast Range Ophiolite, Southwest Oregon: Implications for the Magmatic and Tectonic Evolution of the Coast Range Ophiolite [Ph.D. thesis]: Albany, New York, State University of New York–Albany, 774 p.

Lagabrielle, Y., Roure, F., Coutelle, A., Maury, R.C., Joron, J., and Thonon, P., 1986, The Coast Range ophiolites (Northern California); possible arc and back-arc basin remnants; their relations with the Nevadan orogeny: Bulletin de la Société Geologique de France, Huitième Serie, v. 2, p. 981–999.

Larter, R.D., Vanneste, L.E., Morris, P., and Smythe, D.K., 2003, Structure and tectonic evolution of the South Sandwich arc, *in* Larter, R.D., and Leat, P.T., eds., Intra-Oceanic Subduction Systems; Tectonic and Magmatic Processes: Geological Society [London] Special Publication 219, p. 254–284.

Leat, P.T., Livermore, R.A., Millar, I.L., and Pearce, J.A., 2000, Magma supply in back-arc spreading centre segment E2: East Scotia Ridge: Journal of Petrology, v. 41, p. 845–866, doi: 10.1093/petrology/41.6.845.

Le Maitre, R.W., ed., 2002, Igneous Rocks: A Classification and Glossary of Terms: New York, Cambridge University Press, 263 p.

Livermore, R., 2003, Back-arc spreading and mantle flow in the East Scotia Sea, *in* Larter, R.D., and Leat, P.T., eds., Intra-Oceanic Subduction Systems; Tectonic and Magmatic Processes: Geological Society [London] Special Publication 219, p. 315–331.

MacDonald, J.H., Jr., 2006, Petrology, Petrogenesis, and Tectonic Setting of Jurassic Rocks of the Central Cascades, Washington, and Western Klamath Mountains, California-Oregon, [Ph.D. dissertation]: Albany, University at Albany, 415 p.

MacDonald, J.H., Jr., Harper, G.D., Miller, R.B., and Miller, J.S., 2002, Within-plate magmatic affinities of a lower pillow unit in the Ingalls ophiolite complex, northwest Cascades, Washington: Geological Society of America Abstracts with Programs, v. 34, no. 5, p. 22.

MacDonald, J.H., Jr., Harper, G.D., Miller, R.B., Miller, J.S., and Mlinarevic, A., 2004, Geochemistry and possible tectonic setting of the Esmeralda Peaks unit, and related rocks, Ingalls ophiolite complex, Washington: Geological Society of America Abstracts with Programs, v. 35, no. 5, p. 23.

MacDonald, J.H., Jr., Mlinarevic, A., Harper, G.D., Miller, R.B., Miller, J.S., and Schultz, C.E., 2005, Sedimentary serpentinites of the Ingalls ophiolite complex: Further evidence of a fracture zone setting: Geological Society of America Abstracts with Programs, v. 37, no. 4, p. 86.

MacDonald, J.H., Jr., Harper, G.D., and Zhu, B., 2006, Petrology, geochemistry, and provenance of the Galice Formation, Klamath Mountains, Oregon-California, *in* Snoke, A.W., and Barnes, C.G., eds., Geological Studies in the Klamath Mountains Province, California and Oregon: Geological Society of America Special Paper 410, p. 77–101.

MacDonald, J.H., Jr., Harper, G.D., Miller, R.B., Miller, J.S., and Mlinarevic, A., 2008, this volume, Geochemistry and geology of the Iron Mountain unit, Ingalls ophiolite complex, Washington: Evidence for the polygenetic nature of the Ingalls ophiolite complex, *in* Wright, J.E., and Shervais, J.W., eds., Ophiolites, Arcs, and Batholiths: A Tribute to Cliff Hopson: Geological Society of America Special Paper 438, doi: 10.1130/2008.2438(05).

MacPherson, G.J., 1983, The Snow Mountain volcanic complex; an on-land seamount in the Franciscan terrane, California: The Journal of Geology, v. 91, p. 73–92.

Martinez, F., and Taylor, B., 2003, Controls on back-arc crustal accretion: Insights from the Lau, Manus and Mariana Basins, *in* Larter, R.D., and Leat, P.T., eds., Intra-Oceanic Subduction Systems; Tectonic and Magmatic Processes: Geological Society [London] Special Publication 219, p. 19–54.

Mattinson, J.M., and Hopson, C.A., 1992, U-Pb ages of the Coast Range ophiolite; a critical reevaluation based on new high-precision Pb/Pb ages: American Association of Petroleum Geologists (AAPG) Bulletin, v. 76, no. 3, p. 425.

Matzel, J.P., Bowring, S.A., and Miller, R.B., 2006, Time scales of pluton construction at differing crustal levels: Examples from the Mount Stuart and Tenpeak intrusions, north Cascades, Washington: Geological Society of America Bulletin, v. 118, p. 1412–1430, doi: 10.1130/B25923.1.

McDonough, W.F., and Sun, S.S., 1995, The composition of the Earth: Chemical Geology, v. 120, p. 223–253, doi: 10.1016/0009-2541(94)00140-4.

Menzies, M., Blanchard, D., Brannon, J.C., and Korotev, R., 1977, Rare earth and trace element geochemistry of a fragment of Jurassic seafloor, Point Sal, California: Geochimica et Cosmochimica Acta, v. 41, p. 1419–1430, doi: 10.1016/0016-7037(77)90248-4.

Metzger, E.P., Miller, R.B., and Harper, G.D., 2002, Geochemistry and tectonic setting of the ophiolitic Ingalls complex, north Cascades, Washington; implications for correlations of Jurassic Cordilleran ophiolites: The Journal of Geology, v. 110, p. 543–560, doi: 10.1086/341759.

Miller, J.S., Miller, R.B., Wooden, J.L., and Harper, G.D., 2003, Geochronologic links between the Ingalls ophiolite, north Cascades, Washington, and the Josephine ophiolite, Klamath Mts., Oregon and California: Geological Society of America Abstracts with Programs, v. 35, no. 6, p. 113.

Miller, M.M., and Saleeby, J.B., 1995, U-Pb geochronology of detrital zircon from Upper Jurassic synorogenic turbidites, Galice Formation, and related rocks, western Klamath Mountains; correlation and Klamath Mountains provenance: Journal of Geophysical Research, v. 100, p. 18,045–18,058, doi: 10.1029/95JB00761.

Miller, R.B., 1980, Structure, Petrology and Emplacement of the Ingalls Complex, North-Central Cascade Mountains, Washington [Ph.D. thesis]: Seattle, Washington, University of Washington, 422 p.

Miller, R.B., 1985, The ophiolitic Ingalls Complex, north-central Cascade Mountains, Washington: Geological Society of America Bulletin, v. 96, p. 27–42, doi: 10.1130/0016-7606(1985)96<27:TOICNC>2.0.CO;2.

Miller, R.B., 1988, Fluid flow, metasomatism and amphibole deformation in an imbricated ophiolite, north Cascades, Washington: Journal of Structural Geology, v. 10, p. 283–298, doi: 10.1016/0191-8141(88)90061-2.

Miller, R.B., 1989, The Mesozoic Rimrock Lake Inlier, southern Washington Cascades; implications for the basement to the Columbia Embayment: Geological Society of America Bulletin, v. 101, p. 1289–1305, doi: 10.1130/0016-7606(1989)101<1289:TMRLIS>2.3.CO;2.

Miller, R.B., and Mogk, D.W., 1987, Ultramafic rocks of a fracture-zone ophiolite, north Cascades, Washington: Tectonophysics, v. 142, p. 261–289, doi: 10.1016/0040-1951(87)90127-2.

Miller, R.B., Mattinson, J.M., Goetsch Funk, S.A., Hopson, C.A., and Treat, C.L., 1993, Tectonic evolution of Mesozoic rocks in the southern and central Washington Cascades, *in* Dunne, G.C., and McDougall, K.A.,

eds., Mesozoic Paleogeography of the Western United States: Pacific Section, Society of Economic Paleontologists and Mineralogists, Field Trip Guidebook, part II, v. 71, p. 81–98.

Miller, R.B., Matzel, J.P., Paterson, S.R., and Stowell, H., 2003, Cretaceous to Paleogene Cascades arc, *in* Swanson, T.W., ed., Western Cordillera and Adjacent Areas: Boulder, Colorado, Geological Society of America, Field Guide 4, p. 107–135.

Misch, P., 1966, Tectonic evolution of the northern Cascades of Washington State; a west-Cordilleran case history: Canadian Institute of Mining and Metallurgy, v. 8, Special issue of the Canadian Institute of Mining and Metallurgy, p. 101–148.

Misch, P., 1977, Dextral displacements at some major strike faults in the north Cascades: Geological Association of Canada Programs with Abstracts, v. 2, p. 37.

Miyashiro, A., 1973, The Troodos ophiolite complex probably formed in an island arc: Earth and Planetary Science Letters, v. 19, p. 218–224, doi: 10.1016/0012-821X(73)90118-0.

Mlinarevic, A.N., Miller, R.B., Harper, G.D., MacDonald, J.H., Jr., and Miller, J.S., 2003, Nodal basin (?) sedimentation in an ancient oceanic fracture zone, Ingalls ophiolite complex, Washington: Geological Society of America Abstracts with Programs, v. 35, no. 6, p. 513.

Moore, J.G., 1970, Water content of basalts erupted on the ocean floor: Contributions to Mineralogy and Petrology, v. 28, p. 272–279, doi: 10.1007/BF00388949.

Mottl, M.J., 1983, Metabasalts, axial hot springs, and the structure of hydrothermal systems at mid-ocean ridges: Geological Society of America Bulletin, v. 94, p. 161–180, doi: 10.1130/0016-7606(1983)94<161:MAHSAT>2.0.CO;2.

Murton, B.J., Peate, D.W., Arculus, R.J., Pearce, J.A., and van der Laan, S.R., 1992, Trace element geochemistry of volcanic rocks from Site 786; the Izu-Bonin forearc, *in* Dearmont, L.H., Mazullo, E.K., Stewart, N.J., and Winkler, W.R., et al., Proceedings of the Ocean Drilling Program, Scientific Results 125: College Station, Texas, Ocean Drilling Program, p. 211–235.

Ort, M.H., and Tabor, R.W., 1985, Major- and Trace-Element Composition of Greenstones, Greenschists, Amphibolites, and Selected Mica Schists and Gneisses from the North Cascades, Washington: U.S. Geological Survey Open-File Report 85-434, 12 p.

Palfy, J., Smith, P.L., and Mortensen, J.K., 2000, A U-Pb and $^{40}Ar/^{39}Ar$ time scale for the Jurassic: Canadian Journal of Earth Sciences, v. 37, no. 6, p. 923–944, doi: 10.1139/cjes-37-6-923.

Pearce, J.A., 1982, Trace element characteristics of lavas from destructive plate boundaries, *in* Thorpe, E.S., ed., Andesites: New York, John Wiley and Sons, p. 525–548.

Pearce, J.A., 1996a, A user's guide to basalt discrimination diagrams, *in* Wyman, D.A., ed., Trace Element Geochemistry of Volcanic Rocks; Applications for Massive Sulphide Exploration: Geological Association of Canada, Short Course Notes, v. 12, p. 79–113.

Pearce, J.A., 1996b, Source and setting of granitic rocks: Episodes, v. 19, p. 120–125.

Pearce, J.A., 2003, Supra-subduction zone ophiolites; the search for modern analogues, *in* Dilek, Y., and Newcomb, S., eds., Ophiolite Concept and the Evolution of Geological Thought: Geological Society of America Special Paper 373, p. 269–293.

Pearce, J.A., and Parkinson, I.J., 1993, Trace element models for mantle melting: Application to volcanic arc petrogenesis, *in* Prichard, H.M., et al., eds., Magmatic Processes and Plate Tectonics: Geological Society [London] Special Publication 76, p. 373–403.

Pearce, J.A., and Peate, D.W., 1995, Tectonic implications of the composition of volcanic arc magmas: Annual Review of Earth and Planetary Sciences, v. 23, p. 251, doi: 10.1146/annurev.ea.23.050195.001343.

Pearce, J.A., Lippard, S.J., and Roberts, S., 1984, Characteristics and tectonic significance of supra-subduction zone ophiolites, *in* Kokelaar, B.P., and Howells, M.F., eds., Marginal Basin Geology; Volcanic and Associated Sedimentary and Tectonic Processes in Modern and Ancient Marginal Basins: Geological Society [London] Special Publication 16, p. 74–94.

Pearce, J.A., Thirlwall, M.F., Ingram, G., Murton, B.J., Arculus, R.J., and van der Laan, S.R., 1992, Isotopic evidence for the origin of boninites and related rocks drilled in the Izu-Bonin (Ogasawara) forearc, Leg 125, *in* Fryer, P., Pearce, J.A., et al., Proceedings of the Ocean Drilling Program, Scientific Results, Volume 125: College Station, Texas, Ocean Drilling Program, p. 237–261.

Pearce, J.A., Ernewein, M., Bloomer, S.H., Parson, L.M., Murton, B.J., and Johnson, L.E., 1994, Geochemistry of Lau Basin volcanic rocks: Influence of ridge segmentation and arc proximity, *in* Mellie, J.L., ed., Volcanism Associated with Extension at Consuming Plate Margins: Geological Society [London] Special Publication 81, p. 53–75.

Pearce, J.A., Baker, P.E., Harvey, P.K., and Luff, I.W., 1995, Geochemical evidence for subduction fluxes, mantle melting and fractional crystallization beneath the South Sandwich island arc: Journal of Petrology, v. 36, p. 1073–1109.

Pessagno, E.A., Jr., 1977, Upper Jurassic radiolaria and radiolarian biostratigraphy of the California Coast Ranges: Micropaleontology, v. 23, no. 1, p. 56–113, doi: 10.2307/1485310.

Pessagno, E.A., Jr., 2006, Faunal evidence for the tectonic transport of Jurassic terranes in Oregon, California, and Mexico, *in* Snoke, A.W., and Barnes, C.G., eds., Geological Studies in the Klamath Mountains Province, California and Oregon: Geological Society of America Special Paper 410, p. 31–52.

Pessagno, E.A., Jr., Hull, D.M., Longoria, J.F., and Kelldorf, M.E., 1993, Tectonostratigraphic significance of the San Pedro del Gallo area, Durango, western Mexico, *in* Dunne, G.C., and McDougall, K.A., eds., Mesozoic Paleogeography of the Western United States: Los Angeles, Pacific Section, Society of Economic Paleontologists and Mineralogists, Field Trip Guidebook, part II, p. 141–156.

Pessagno, E.A., Jr., Hull, D.M., and Hopson, C.A., 2000, Tectonostratigraphic significance of sedimentary strata occurring within and above the Coast Range ophiolite (California Coast Ranges) and the Josephine ophiolite (Klamath Mountains), northwestern California, *in* Dilek, Y., Moores, E.M., Elthon, D., and Nicolas, A., eds., Ophiolites and Oceanic Crust: New Insights from Field Studies and the Ocean Drilling Program: Geological Society of America Special Paper 349, p. 383–394.

Pinto-Auso, M., and Harper, G.D., 1985, Sedimentation, metallogenesis, and tectonic origin of the basal Galice Formation overlying the Josephine ophiolite, northwestern California: The Journal of Geology, v. 93, p. 713–725.

Plank, T., and Langmuir, C.H., 1993, Tracing trace elements from sediment input to volcanic output at subduction zones: Nature, v. 362, p. 739–743, doi: 10.1038/362739a0.

Pratt, R.M., 1958, Geology of the Mt. Stuart Area, Washington [Ph.D. thesis]: Seattle, Washington, University of Washington, 203 p.

Robertson, A.H.F., 1990, Sedimentology and tectonic implications of ophiolite-derived clastics overlying the Jurassic Coast Range ophiolite, northern California: American Journal of Science, v. 290, p. 109–163.

Saleeby, J.B., 1984, Pb/U zircon ages from the Rogue river area, Western Jurassic belt, Klamath Mountains, Oregon: Geological Society of America Abstracts with Programs, v. 16, no. 5, p. 331.

Saleeby, J.B., 1990, Geochronological and tectonostratigraphic framework of Sierran-Klamath ophiolitic assemblages, *in* Harwood, D.S., and Miller, M.M., eds., Paleozoic and Early Mesozoic Paleogeographic Relations: Sierra Nevada, Klamath Mountains, and Related Terranes: Geological Society of America Special Paper 255, p. 93–114.

Saleeby, J.B., 1992, Petrotectonic and paleogeographic settings of the U.S. Cordilleran ophiolites, *in* Burchfiel, B.C., et al., eds., The Cordilleran Orogen: Conterminous U.S.: Boulder, Colorado, Geological Society of America, Geology of North America, v. G-3, p. 653–683.

Saleeby, J.B., Harper, G.D., Snoke, A.W., and Sharp, W.D., 1982, Time relations and structural-stratigraphic patterns in ophiolite accretion, west central Klamath Mountains, California: Journal of Geophysical Research, v. 87, p. 3831–3848.

Schultz, C.E., Miller, R.B., Miller, J.S., and MacDonald, J.H., Jr., 2005, Mantle peridotites in the Ingalls ophiolite: Geological Society of America Abstracts with Programs, v. 37, no. 4, p. 85.

Seyfried, W.E., Jr., 1987, Experimental and theoretical constraints on hydrothermal alteration processes at mid-ocean ridges: Annual Review of Earth and Planetary Sciences, v. 15, p. 317–335, doi: 10.1146/annurev.ea.15.050187.001533.

Shervais, J.W., 1982, Ti-V plots and the petrogenesis of modern and ophiolitic lavas: Earth and Planetary Science Letters, v. 59, p. 101–118, doi: 10.1016/0012-821X(82)90120-0.

Shervais, J.W., 1990, Island arc and ocean crust ophiolites: Contrasts in the petrology, geochemistry, and tectonic style of ophiolite assemblages in the California Coast Ranges, *in* Malpas, J., Moores, E.M., Panayiotou, A., and Xenophontos, C., eds., Ophiolites: Oceanic Crustal Analogues, Pro-

ceedings of the Symposium Troodos 1987: Nicosia, Cyprus, The Geological Survey Department, Minstry of Agriculture and Natural Resources, p. 507–520.

Shervais, J.W., 2001, Birth, death, and resurrection; the life cycle of suprasubduction zone ophiolites: Geochemistry, Geophysics, Geosystems, v. 2, doi: 10.1029/2000GC000080.

Shervais, J.W., and Kimbrough, D.L., 1985, Geochemical evidence for the tectonic setting of the Coast Range ophiolite; a composite island arc–oceanic crust terrane in western California: Geology, v. 13, no. 1, p. 35–38, doi: 10.1130/0091-7613(1985)13<35:GEFTTS>2.0.CO;2.

Shervais, J.W., Murchey, B., Kimbrough, D.L., Hanan, B.B., Renne, P.R., Snow, C.A., Schuman, M.Z., and Beaman, J., 2004, Multi-stage origin of the Coast Range ophiolite, California: Implications for the life cycle of supra-subduction zone ophiolites: International Geology Review, v. 46, p. 289–315.

Shervais, J.W., Murchey, B., Kimbrough, D.L., Renne, P.R., and Hanan, B.B., 2005a, Radioisotopic and biostratigraphic age relations in the Coast Range ophiolite, northern California: Implications for the tectonic evolution of Western Cordillera: Geological Society of America Bulletin, v. 117, p. 633–653, doi: 10.1130/B25443.1.

Shervais, J.W., Schuman, M.M.Z., and Hanan, B.B., 2005b, The Stonyford volcanic complex: A forearc seamount in the northern California Coast Ranges: Journal of Petrology, v. 46, p. 2091–2128, doi: 10.1093/petrology/egi048.

Sinton, J.M., Wilson, D.S., Christie, D.M., Hey, R.N., and Delaney, J.R., 1983, Petrologic consequences of rift propagation on ocean spreading ridges: Earth and Planetary Science Letters, v. 62, p. 193–207, doi: 10.1016/0012-821X(83)90083-3.

Smith, G.O., 1904, Description of the Mount Stuart Quadrangle: U.S. Geological Survey Atlas, Mount Stuart folio, no. 106, 10 p.

Smith, S.E., 1994, Geochemistry and Petrology of Basaltic and Plutonic Rocks from the Hayes Transform Region, Mid-Atlantic Ridge [Ph.D. thesis]: Houston, Texas, University of Houston, 309 p.

Snoke, A.W., 1977, A thrust plate of ophiolitic rocks in the Preston Peak area, Klamath Mountains, California: Geological Society of America Bulletin, v. 88, p. 1641–1659, doi: 10.1130/0016-7606(1977)88<1641:ATPOOR>2.0.CO;2.

Southwick, D.L., 1962, Mafic and Ultramafic Rocks of the Ingalls-Peshastin Area, Washington, and Their Geologic Setting [Ph.D. thesis]: Baltimore, Maryland, Johns Hopkins University, 287 p.

Southwick, D.L., 1974, Geology of the alpine-type ultramafic complex near Mount Stuart, Washington: Geological Society of America Bulletin, v. 85, p. 391–402, doi: 10.1130/0016-7606(1974)85<391:GOTAUC>2.0.CO;2.

Stern, R.J., 2002, Subduction zones: Review of Geophysics, v. 40, doi: 10.1029/2001RG000108.

Stern, R.J., and Bloomer, S.H., 1992, Subduction zone infancy; examples from the Eocene Izu-Bonin-Mariana and Jurassic California arcs: Geological Society of America Bulletin, v. 104, p. 1621–1636, doi: 10.1130/0016-7606(1992)104<1621:SZIEFT>2.3.CO;2.

Sun, S.S., and McDonough, W.F., 1989, Chemical and isotopic systematics of oceanic basalts; implications for mantle composition and processes, *in* Saunders, A.D., and Norry, M.J., eds., Magmatism in the Ocean Basins: Geological Society [London] Special Publication 42, p. 313–345.

Tabor, R.W., 1994, Late Mesozoic and possible early Tertiary accretion in western Washington State: The Helena-Haystack mélange and the Darrington–Devils Mountain fault zone: Geological Society of America Bulletin, v. 106, p. 217–232, doi: 10.1130/0016-7606(1994)106<0217:LMAPET>2.3.CO;2.

Tabor, R.W., Waitt, R.B., Jr., Frizzell, V.A., Jr., Swanson, D.A., Byerly, G.R., and Bentley, R.D., 1982, Geologic Map of the Wenatchee 1:100,000 Quadrangle, Central Washington: U.S. Geological Survey Miscellaneous Investigations Series I-1311, 26 p.

Tabor, R.W., Frizzell, V.A., Jr., Whetten, J.T., Waitt, R.B., Jr., Swanson, D.A., Byerly, G.R., Booth, D.B., Hetherington, M.J., and Zartman, R.E., 1987, Geologic Map of the Chelan 30′ by 60′ Quadrangle, Washington: U.S. Geological Survey Miscellaneous Investigations Series I-1661, 33 p.

Tabor, R.W., Frizzell, V.A., Jr., Booth, D.B., Waitt, R.B., Whetten, J.T., and Zartman, R.E., 1993, Geologic Map of the Skykomish River 30′ by 60′ Quadrangle, Washington: U.S. Geological Survey Miscellaneous Investigations Series I-1963, 42 p.

Tabor, R.W., Frizzell, V.A., Jr., Booth, D.B., and Waitt, R.B., 2000, Geologic Map of the Snoqualmie Pass 30′ by 60′ Quadrangle, Washington: U.S. Geological Survey Geologic Investigations Series I-2538, 57 p.

Tartarotti, P., Cannat, M., and Mevel, C., 1995, Gabbroic dikelets in serpentinized peridotites from the Mid-Atlantic Ridge at 23°20′N, *in* Vissers, R.L.M., and Nicolas, A., eds., Mantle and Lower Crust Exposed in Oceanic Ridges and in Ophiolites: Netherlands, Kluwer Academic Publishers, p. 35–69.

Van der Laan, S.R., Flower, M.F.J., and Koster van Groos, A.F., 1989, Experimental evidence for the origin of boninites; near-liquidus phase relations to 7.5 kbar, *in* Crawford, A.J., ed., Boninites: London, Unwin Hyman, p. 112–147.

Whetten, J.T., Jones, D.L., Cowan, D.S., and Zartman, R.E., 1978, Ages of Mesozoic terranes in the San Juan Islands, Washington, *in* Howell, D.G., and McDougall, K., eds., Mesozoic Paleogeography of the Western United States: Los Angeles, Society of Economic Paleontologists and Mineralogists, Pacific Section, p. 117–132.

Whetten, J.T., Zartman, R.E., Blakely, R.J., and Jones, D.L., 1980, Allochthonous Jurassic ophiolite in northwest Washington: Geological Society of America Bulletin, v. 91, p. 359–368, doi: 10.1130/0016-7606(1980)91<359:AJOINW>2.0.CO;2.

Wood, D.A., 1980, The application of a Th-Hf-Ta diagram to problems of tectonomagmatic classification and to establishing the nature of crustal contamination of basaltic lavas of the British Tertiary Volcanic Province: Earth and Planetary Science Letters, v. 50, p. 11–30, doi: 10.1016/0012-821X(80)90116-8.

Wright, J.E., and Wyld, S.J., 1986, Significance of xenocrystic Precambrian zircon contained within the southern continuation of the Josephine ophiolite: Devils Elbow ophiolite remnant, Klamath Mountains, Northern California: Geology, v. 14, no. 8, p. 671–674, doi: 10.1130/0091-7613(1986)14<671:SOXPZC>2.0.CO;2.

Wright, J.E., and Wyld, S.J., 1994, The Rattlesnake Creek terrane, Klamath Mountains, California: An early Mesozoic volcanic arc and its basement of tectonically disrupted oceanic crust: Geological Society of America Bulletin, v. 106, p. 1033–1056, doi: 10.1130/0016-7606(1994)106<1033:TRCTKM>2.3.CO;2.

Wyld, S.J., and Wright, J.E., 1988, The Devils Elbow ophiolite remnant and overlying Galice Formation: New constraints on the Middle to Late Jurassic evolution of the Klamath Mountains, California: Geological Society of America Bulletin, v. 100, p. 29–44, doi: 10.1130/0016-7606(1988)100<0029:TDEORA>2.3.CO;2.

Wyld, S.J., Umhoefer, P., and Wright, J.E., 2006, Reconstructing northern Cordilleran terranes along known Cretaceous and Cenozoic strike-slip faults: Implications for the Baja B.C. hypothesis and other models, *in* Monger, J., Enkin, R., and Haggert, J., eds., Paleogeography of the North American Cordillera: Evidence For and Against Large-Scale Displacements: Geological Association of Canada Special Paper, p. 277–298.

Yule, J.D., Saleeby, J.B., and Barnes, C.G., 2006, A rift-edge facies of the Late Jurassic Rogue-Chetco arc and Josephine ophiolite, Klamath Mountains, Oregon, *in* Snoke, A.W., and Barnes, C.G., eds., Geological Studies in the Klamath Mountains Province, California and Oregon: Geological Society of America Special Paper 410, p. 53–76.

Manuscript Accepted by the Society 16 July 2007